Lawrence Berkeley National Laboratory

Recent Work

Title

Properties and Applications of Amorphous Silicon in Charged Particle, Gamma Ray and Light Detection

Permalink

https://escholarship.org/uc/item/4cd8161g

Authors

Perez-Mendez, V.
Cho, G.
Drewery, J.
et al.

Publication Date

1990-02-01

eScholarship.org Powered by the California Digital Library
University of California

UC-411

LBL-28339

Lawrence Berkeley Laboratory

UNIVERSITY OF CALIFORNIA

Physics Division

To be published as a chapter in **Physics and Applications of Amorphous and Microcrystalline Semiconductor Devices**, J. Kanicki, Ed., Artech House, Boston, MA, Fall 1990

Properties and Applications of Amorphous Silicon in Charged Particle, Gamma Ray and Light Detection

V. Perez-Mendez, G. Cho, J. Drewery, I. Fujieda, S.N. Kaplan, S. Qureshi, and R.A. Street

February 1990

For Reference

Not to be taken from this room

Prepared for the U.S. Department of Energy under Contract Number DE-AC03-76SF00098.

LBL-28339
Copy 1
Bldg. 50 Library.

DISCLAIMER

This document was prepared as an account of work sponsored by the United States Government. While this document is believed to contain correct information, neither the United States Government nor any agency thereof, nor the Regents of the University of California, nor any of their employees, makes any warranty, express or implied, or assumes any legal responsibility for the accuracy, completeness, or usefulness of any information, apparatus, product, or process disclosed, or represents that its use would not infringe privately owned rights. Reference herein to any specific commercial product, process, or service by its trade name, trademark, manufacturer, or otherwise, does not necessarily constitute or imply its endorsement, recommendation, or favoring by the United States Government or any agency thereof, or the Regents of the University of California. The views and opinions of authors expressed herein do not necessarily state or reflect those of the United States Government or any agency thereof or the Regents of the University of California.

LBL-28339

Properties and Applications of Amorphous Silicon in Charged Particle, Gamma Ray and Light Detection

V. Perez-Mendez, G. Cho, J. Drewery, I. Fujieda,
S.N. Kaplan, S. Qureshi

Lawrence Berkeley Laboratory
University of California
Berkeley, CA 94720

and

R.A. Street

Xerox
Palo Alto Research Laboratory
Palo Alto, CA 94306

February 1990

This work was supported by the Director, Office of Energy Research,
Office of High Energy and Nuclear Physics, Division of High Energy Physics
of the U. S. Department of Energy under Contract No. DE-AC03-76SF00098.

LBL 28339

PROPERTIES AND APPLICATIONS OF AMORPHOUS SILICON IN CHARGED PARTICLE, GAMMA RAY AND LIGHT DETECTION

V. Perez-Mendez, G. Cho, J. Drewery, I. Fujieda, S. N. Kaplan, S. Qureshi, Lawrence Berkeley Laboratory, University of California, Berkeley, CA 94720
R. A. Street, Xerox, Palo Alto Research Laboratory, Palo Alto, CA 94306

1 INTRODUCTION

Crystalline semiconductors such as silicon and germanium have had a long record of functioning as detectors of ultraviolet and visible light, charged particles, x-rays and γ rays. In this paper we cover similar uses of a-Si:H diodes for these applications, emphasizing the similarities and differences in the device structures and the modifications imposed by the unique properties of a-Si:H.

A solid state detector for any form of radiation is a reverse biased diode. The incident radiation liberates a number of electron-hole pairs which are subsequently drifted to the boundary contacts and collected there. A basic requirement for a detector diode is that the background noise produced in the absence of incident radiation should be adequately smaller than the radiation produced signal.

The incident radiation can be detected as a fluence in some cases. Alternatively, other applications require the detection of individual high energy photons (x-rays, γ rays) or individual charged particles. In applications involving single photon or single particle detection the energy deposited in the diode layer is collected as a charge. In some cases, the position and transit time of each particle is of interest and recorded as such by the configuration of the detector structure and its associated detecting electronics. Position sensitive devices of this type often consist of a large area detector subdivided into strips or small areas (pixels). In a few applications it is necessary to record event by event the energy deposited in the detector as well as the position. Usually this does not require a different detector structure only different electronic readout devices.

Two basic detector configurations are shown schematically in Fig. 1. These are reverse biased *p-i-n* diodes in which thin ~ 30 nm p^+ and n^+ layers are deposited on the electrodes and the bulk of the material is the *i* layer. Fig. 1a shows such a detector in which the *i* layer is made 30-100μm thick in order for incident charged particles to be able to deposit enough energy to produce a large enough signal. Fig. 1b shows an alternative configuration in which a thin 1-2μm thick *p-i-n* diode acts as a detector of visible light and is coupled to a thick (>100μm) converter layer of CsI or some other scintillator which

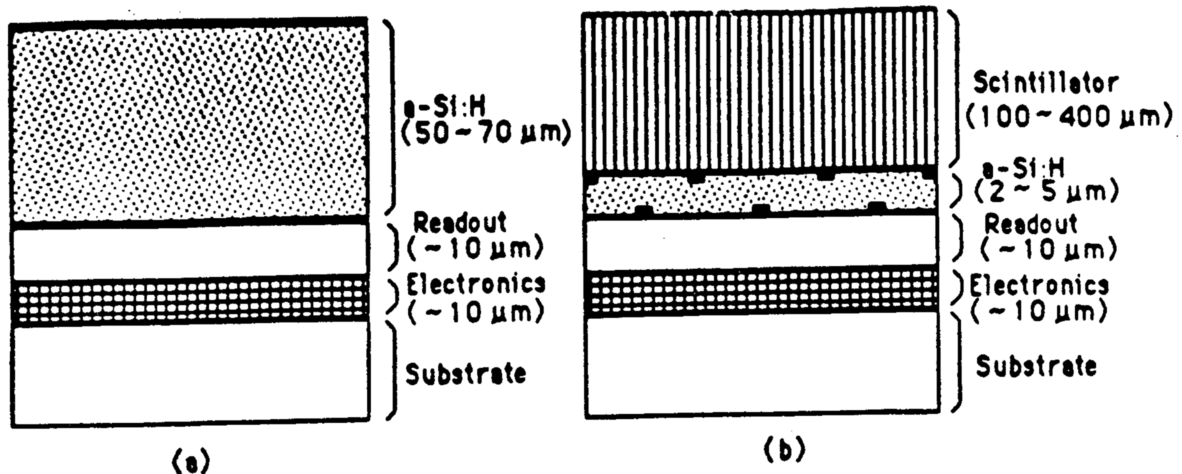

Fig. 1: a-Si:H detector schemes coupled to readout electronics. (a) Thick (50μm) fully depleted *p-i-n* layer. For direct detection of charged particles. (b) Thin (2μm) *p-i-n* layer to detect visible light from scintillator converter.

converts the energy deposited by charged particles, x-rays or γ-rays into light in the visible range (~400-700nm). The signal in both cases is $V = Q/C$ where Q is the collected charge and C the electrical capacity of the detector element. For single particle detection where Q is often in the range of only a few thousand *e*, *h* pairs, the detector capacitance should be kept to a minimum in order to achieve a large signal to noise ratio.

A conventional circuit which is often used with XTAL Si detectors and can be used here as well is shown in Fig. 2. It consists of a charge sensitive low noise amplifier which is an operational amplifier with a small capacitance feed back loop which collects the charge and produces a voltage output $V \sim Q/C_f$. Details of signal amplification and noise are covered in Sect.7.

2. PROPERTIES OF DETECTOR DIODES

The requirement for a thick, fully depleted *i* layer poses some difficulties for the a-Si:H diodes which are not present in the Xtal Si case. The *i* layer has a density of neutral dangling bonds which release electrons when a sufficient bias voltage is applied. The

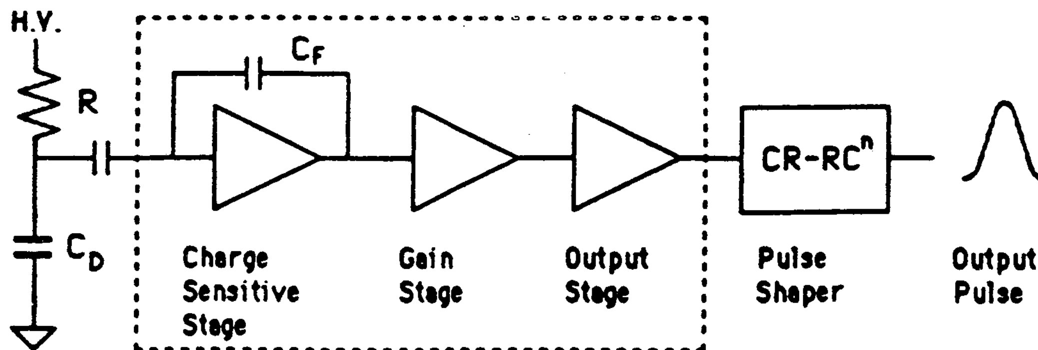

Fig. 2: Conventional electronics for detection of small signals from semiconductor detectors. Three stage amplifier in proximity to detector is followed by shaping circuit.

residual positive charge density ρ left behind modifies the electric field of the bias voltage so that the *i* region has an electric field gradient.

This electric field, for a planar detector, can be calculated from a one dimensional Poisson equation following [1]. We divide the *i* layer into two contiguous regions. In region I, where V(x) is greater than a critical voltage V_c, the charge density is taken to be a constant $\rho_0 = +qN_D^*$ where q = charge of the electron and N_D^* = density of ionized dangling bonds.

The Poisson equation has the form

$$\frac{d^2V}{dx^2} = \frac{-\rho_0}{\varepsilon\varepsilon_0} \qquad - (1)$$

When the potential V(x) drops below V_c we assume $\rho = \rho_0 V(x) / \varepsilon\varepsilon_0 V_c$. Hence the

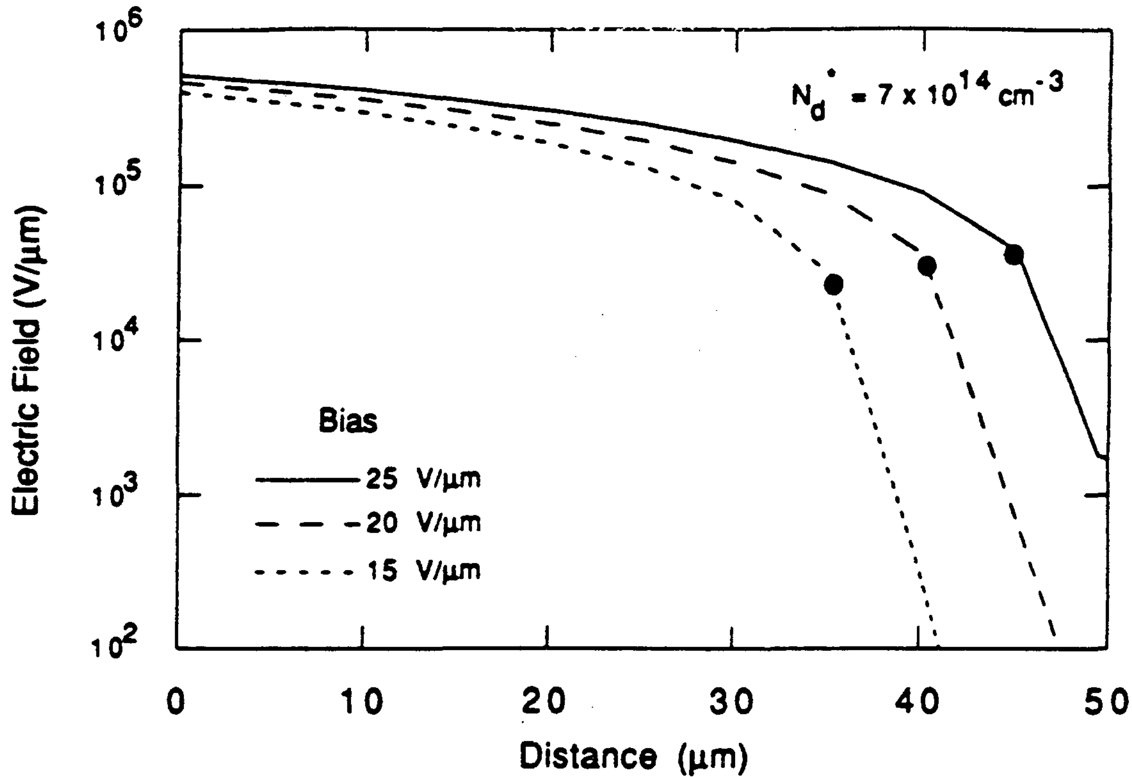

Fig. 3: Electric field vs. distance in 50µm *p-i-n* detector, calculated for different bias voltages. Black dots indicate position of V_c = 1V.

Poisson equation in region II becomes

$$\frac{d^2V}{dx^2} = \frac{-\rho_0}{\varepsilon\varepsilon_0}\frac{V(x)}{V_c} \qquad - (2)$$

The equations are solved [2] (see Appendix A) assuming the boundary condition for a layer of thickness d. $V(0) = V_{bias}$, $V(d) = 0$ and continuity of V and dV/dx at the boundary between regions I and II. V_c is taken to be 1 volt. With these conditions the solution in region I for the electric field is linear with a slope $\rho_0 / \varepsilon\varepsilon_0$ with maximum value at the *p-i* interface. In region II the electric field is approximately exponential with exponent $-\sqrt{\rho_0 / V_c \varepsilon\varepsilon_0}\ x$.

In order to minimize electric field gradients, the density of dangling bonds should be kept to a minimum level. It has been shown [3] that N_D^* (density of ionized dangling bonds) ~ 0.3 N_D where N_D=total dangling bond density. At present the lowest dangling bond density produced in intrinsic a-Si:H by standard PECVD reactors operating at 13.5 MHz is ~ 1-2x10^{15}/cm^3 as measured by conventional electron spin resonance techniques.

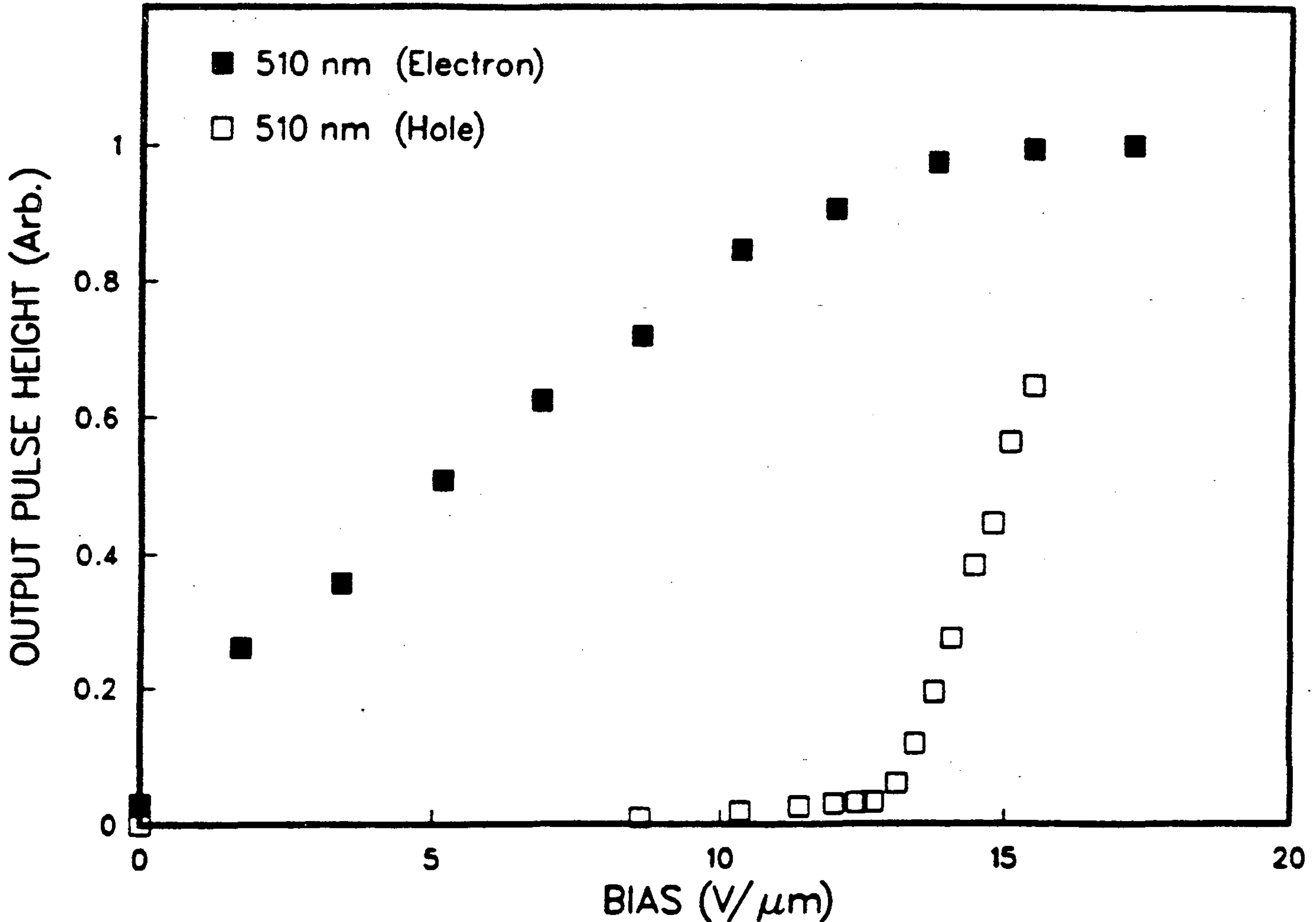

Fig. 4: Output signal from 510nm light incident on *n* and *p* contacts of 29 μm pin diode. Threshold signal for hole collection at V=13V/μm bias indicates full depletion.

The electric field calculated from the Poisson equation for an assumed value $N_D^* \sim 7 \times 10^{14}/cm^3$ is shown in Fig. 3. Thus in order to fully deplete a *p-i-n* diode with *i* layer 50μm thick a bias voltage >20V/μm is required.

The requirement for full depletion is also shown in Fig. 4 where the response to a pulsed light source λ=510nm incident on the *p* and *n* sides of the diode is shown. The absorption mean free path for λ=510nm light is <0.3 μm. Hence, when the light is incident on the *p* side the electrons traverse the full thickness of the *i* layer until they are collected. They experience an electric field which peaks at the *p-i* interface and drops off with distance. When the light is incident on the *n* side the holes have to traverse the entire *i* layer. However, hole collection does not start until the electric field as a function of bias voltage becomes sufficiently large to drift the holes at the *i-n* interface. This threshold value for the E field as calculated from Fig. 4 at a bias of 13V/μm is ~500V/cm; at this point the *p-i-n* diode is fully depleted, and the hole signal increases from zero as shown.

2.1 Field Shaping in *i* Layer

The fact that the electric field peaks at the *p-i* interface close to the metal contact

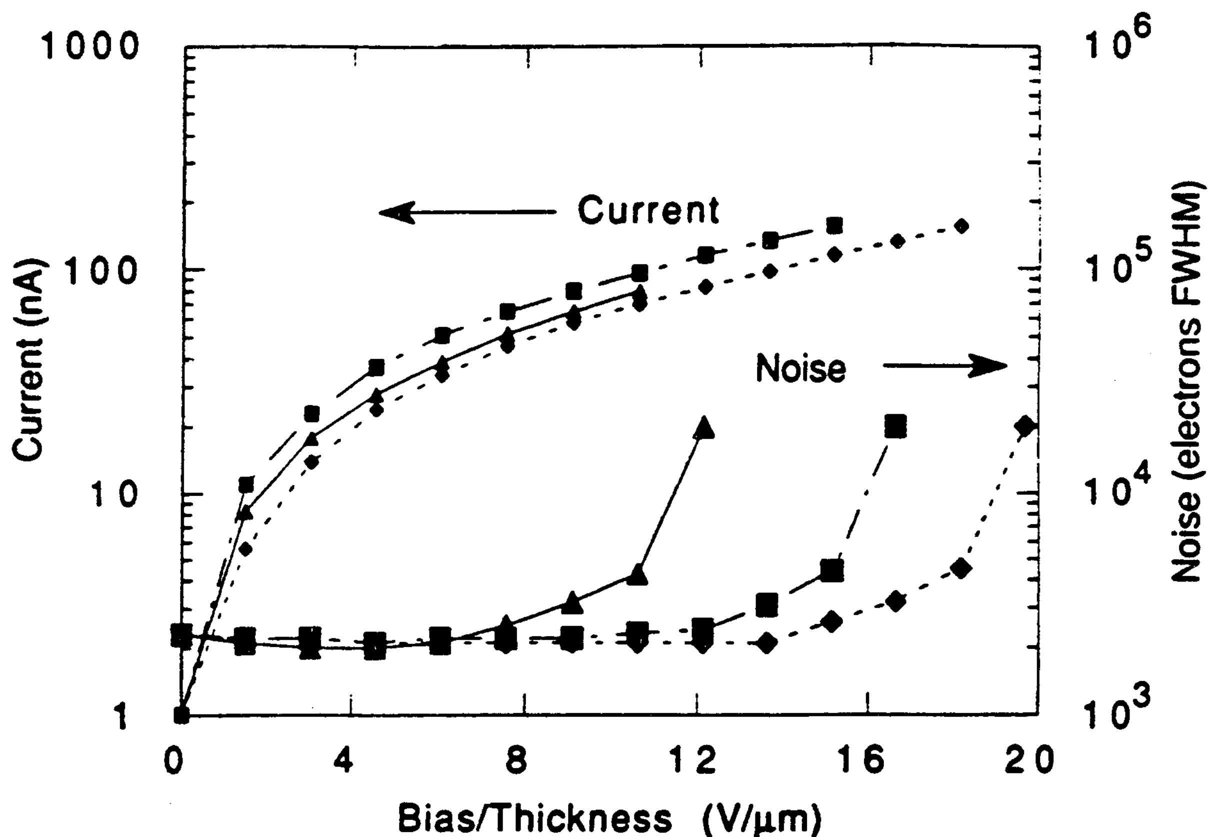

Fig. 5: Reverse bias currents and noise for three *p-i-n* diodes. Position of rapid noise increase indicates start of microplasma breakdown.

limits the maximum bias which can be applied before some breakdown occurs. The existence of a breakdown level can be seen in three diodes in Fig. 5 in which the noise increases rapidly at a specific bias. This breakdown may be due to some microplasma discharge at the metal p^+-*i* interface [4].

Two methods for achieving higher E fields in the *i* layer by permitting the use of higher bias potential without breakdown are shown in Figs. 6 and 9. In Fig. 6, thin *p* and

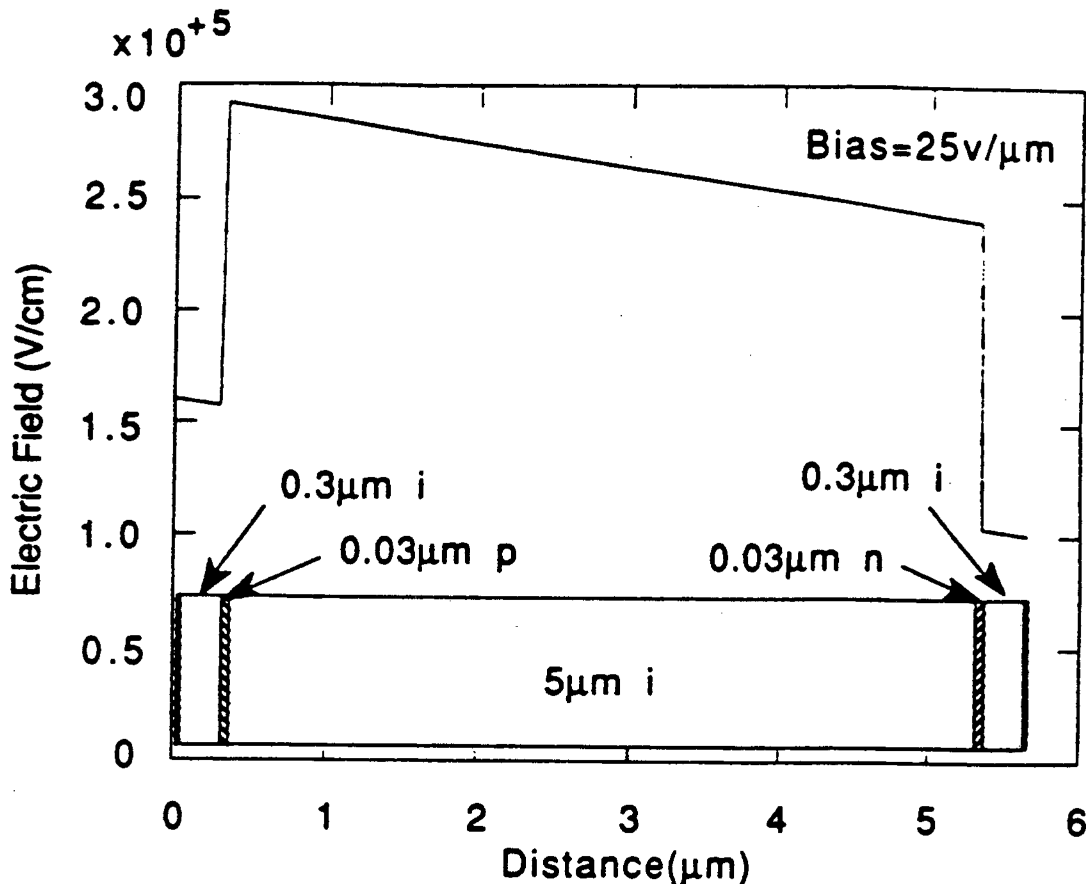

Fig. 6: Electric field vs. distance in 5.6µm *p-i-n* detector with 'buried' *p* and *n* layers. The density of electrically active *p* and *n* dopants is $3 \times 10^{17}/cm^3$.

n layers are placed within the *i* layer which modify the electric field near the *p* metal surface [5]. This is calculated using the Poisson equation with the right boundary conditions, i.e. continuity of V, dV/dx at each interface. Since an ionized *p* layer produces a fixed -ve charge, the electric field drops within it. Here we assume for the *p* layer a charge density $\rho = -|q|.n_a$ where $n_a = 3 \times 10^{17}/cm^3$. This concentration of electrically active boron dopant can be achieved by using a mixture of $SiH_4 + B_2H_6$ (10^{-4} concentration in gas) in the PECVD reactor [6]. A similar concentration of *n* dopant is achieved by the use of $SiH_4 + PH_3(10^{-4})$. The effectiveness of this scheme is shown in Fig. 7. The permissible bias voltage rises up to 50V/µm before the onset of breakdown. The bar graphs - Fig. 8 - show

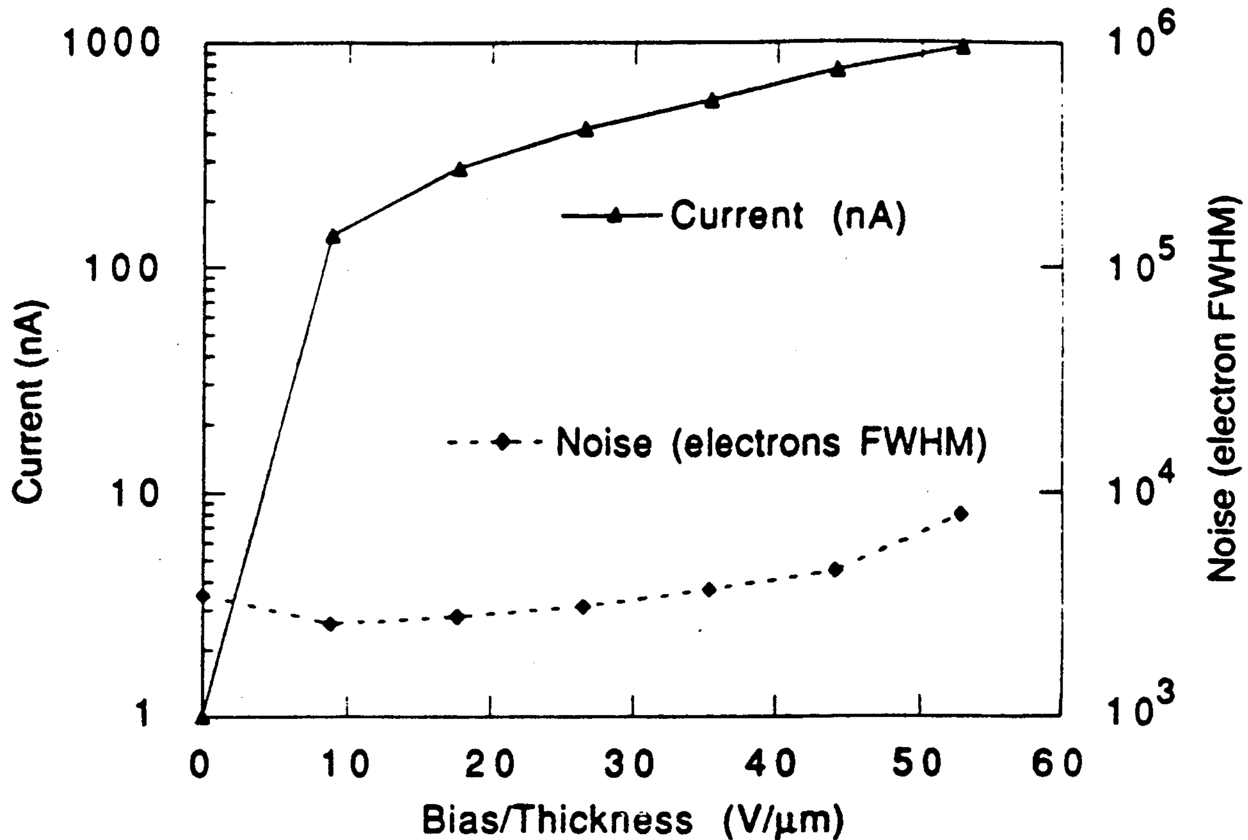

Fig. 7: Reverse current and noise in 5.6μm *p-i-n* detector with thin buried *p* and *n* layers. Breakdown level raised to 55 V/μm bias.

that *p-i-n* diodes with buried *p* layers systematically can withstand higher bias potentials before the onset of microplasma breakdown than the conventional p^+-i-n^+ diodes.

A second method for accomplishing this objective is to make the p^+ layer thicker [7]. Fig. 9 shows the electric fields calculated for a 200nm *p* layer with a concentration of electrically active boron = $3 \times 10^{17}/\mathrm{cm}^3$. Another desirable objective - which is to decrease the overall applied bias required for full *i* layer depletion and to decrease the range of E fields within the *i* layer - can be achieved [8] by placing one *p* layer in the central region of the *i* layer as shown in Fig. 9. Further reduction in bias potential and a more uniform electric field can be achieved with two central *p* layers as shown in Fig. 10.

The integrated amount of *p* doping that is acceptable in such layers is limited by the fact that electrons have considerably decreased μτ values in the *p* doped layer, whereas holes are essentially unaffected [9]. A calculation based on a value $(\mu\tau)_e = 5 \times 10^{-10}\ \mathrm{cm}^2/\mathrm{v}$ shows that we lose less than 10% of the electrons in traversing such layers.

A third field shaping situation arises in the case of the thin *i* layer (1-2μm) *p-i-n* diodes mentioned previously as visible light detectors. For single event detection the electrical capacitance can be reduced by the use of interdigitated electrodes and their resultant equipotential lines as shown in Fig. 11. From the figure and the *i*layer distance

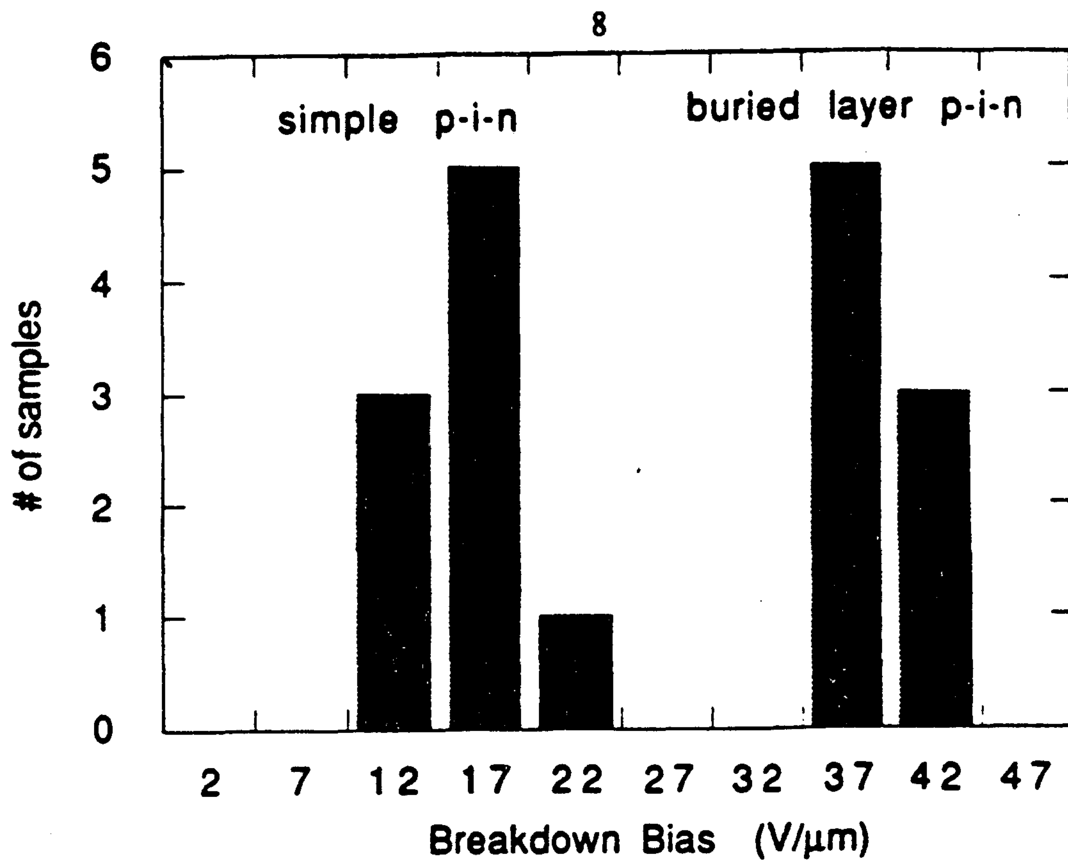

Fig. 8: Bar graph showing comparison in breakdown levels for simple and buried layer *p-i-n* diodes.

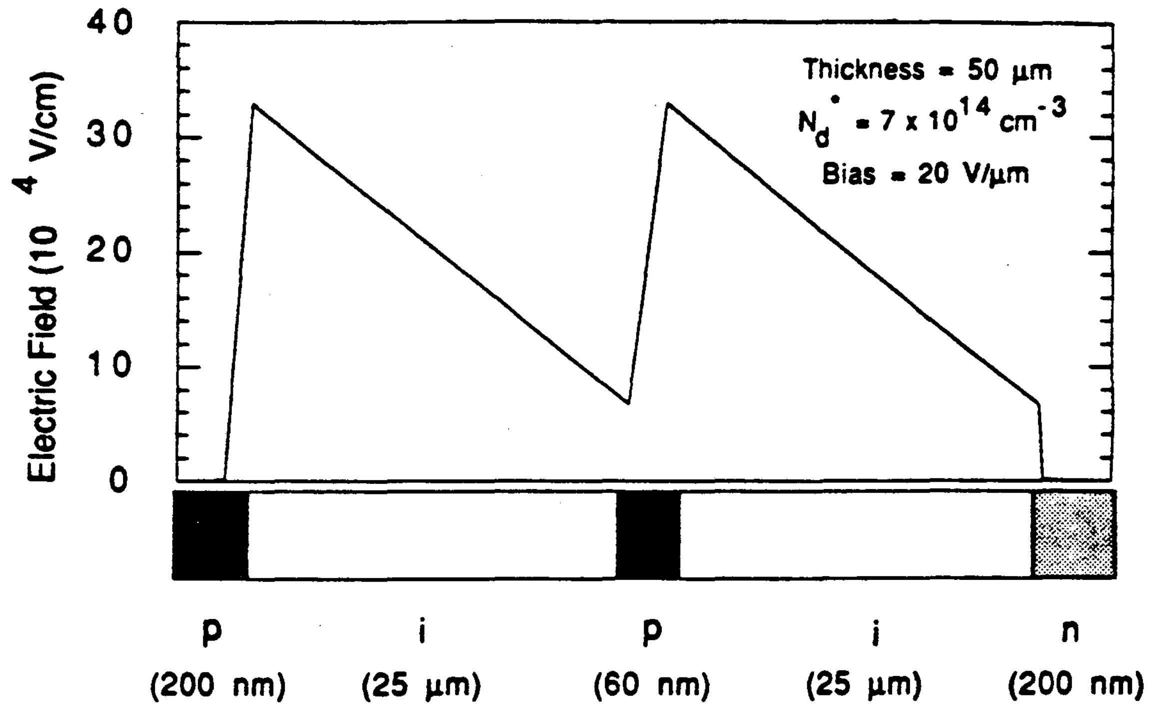

Fig. 9: Electric field in 50µm *p-i-n* diode with 200nm thick *p* and *n* doped layers adjacent to metal contacts. One central *p* layer 60nm thick improves average E field slope. All doped layers have 3 x 10^{17}/cm^3 electrically active dopants.

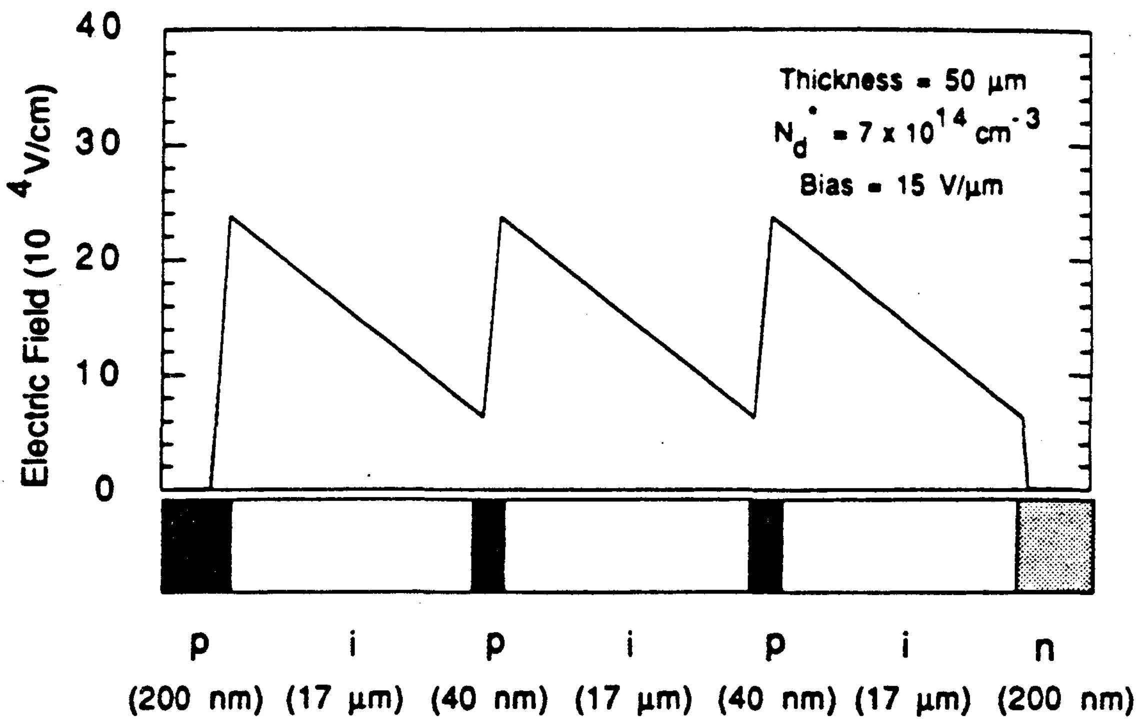

Fig. 10: Electric field in 50μm *p-i-n* diode with 200nm thick *p*, *n* layers adjacent to contacts. Two buried *p* layers in bulk of *i* material permit full depletion at bias of 15V/μm.

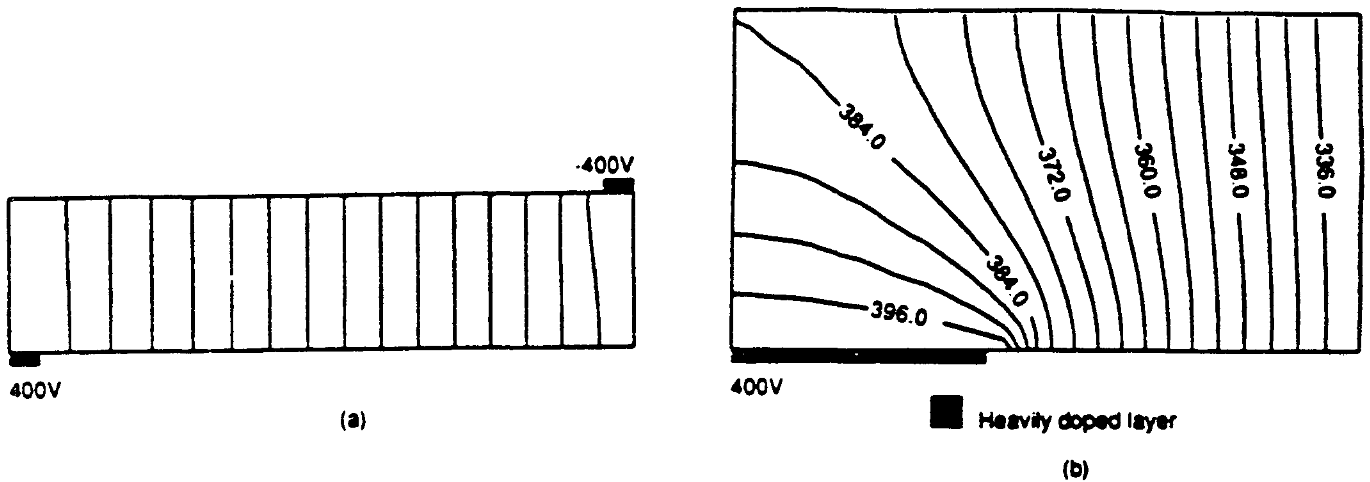

Fig. 11: Interdigitated electrode diode configuration for low capacitance detection of scintillation light. (a) Equipotentials. (b) Equipotentials near *n* contact.

from electrode to electrode, it is apparent that high biases would have to be applied, with a resultant high E field at the *p-i* interface; it is therefore desirable to use the buried or thick *p* region schemes shown in Fig. 6 and Fig. 9. The top metal and *p* layers can be etched away in the same etching operation, to produce the resultant configuration shown here. The

capacitance of this diode is 25 pF/cm^2 compared to 5300 pF/cm^2 for the parallel electrode structure.

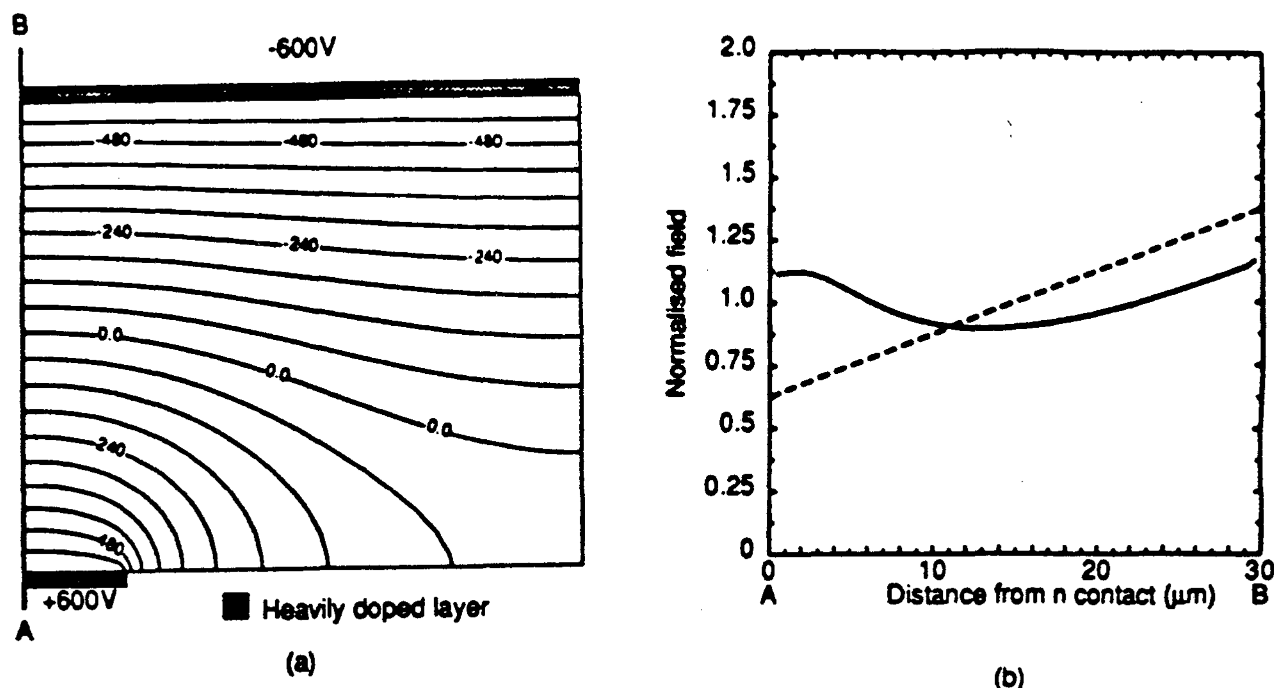

Fig. 12: Continuous *p* and spaced out *n* electrode for field enhancement diode. (a) Equipotentials lines. (b) Electric field in Section A-B showing E field for parallel and shaped electrode cases.

A fourth field shaping scheme [10] which reduces the difference in E field values between the high field at the *p-i* interface and the minimal full depletion field at the *i-n* interface is shown schematically in Fig. 12. The negative electrode consists of a continuous metallic layer with a conventional p^+ layer or a 200nm p (3×10^{17}/cm^3) layer followed by the bulk *i* layer. The +ve contacts consist of spaced metallic electrodes above a thin n^+ layer. The geometrical increase of $|E|$ due to the electrode configuration compensates to some extent for the decrease in $|E|$ due to the ionized dangling bonds in the *i* layer. Fig. 12b shows the values of E fields with continuous and with spaced out -ve electrodes for the case of a 30μm thick *i* layer with $N_d^* \sim 7 \times 10^{14}$/cm^3. This scheme also has the advantage of reducing the detector capacitance from 354 pF/cm^2 to 85 pF/cm^2.

3 LIGHT DETECTION IN a-Si:H DETECTORS

While it is in principle possible to detect x-rays directly in an amorphous silicon *p-i-n* device, it is also possible to use an indirect detection method which utilizes a scintillating material such as CsI as the primary x-ray detector, the light from the scintillations being detected by an amorphous silicon diode array. In this way a considerably larger signal can

be expected than if the x-ray had been detected directly. This argument applies to any form of radiation for which a good scintillator is available. One therefore requires a detector optimized for the most efficient detection of scintillation light.

Amorphous silicon is widely studied and manufactured as a material for the fabrication of photovoltaic cells for power generation. It is certainly feasible to use a-Si:H to detect light; however, the factors which must be taken into account in the design of such detectors differ from the case of solar cells. Solar cells are intended to provide the maximum power output when continuously illuminated by sunlight, which has a broad spectrum. Such parameters as the short circuit current and the 'fill factor' (the ratio of maximum power available to the product of the short circuit current and the open circuit voltage) determine the suitability of a device. A detector for use in conjunction with some scintillator need be optimized only for light of the wavelengths emitted by the scintillator, and for the particular amplification circuitry to be used. The low light levels to be detected make the average photocurrent yields to be expected considerably smaller than the values of leakage current found in reverse bias *p-i-n* detectors to date. While it may be that future improvements in design and in materials will make it possible to use DC amplification, at present it is envisaged that counting of individual scintillations, with the associated pulse amplification and shaping circuitry, will be necessary.

3.1 The Light Absorption Mechanism

Crystalline silicon is an indirect gap semiconductor. In order for an electron transition from the valence band maximum to the conduction band minimum to occur, an interaction with both a photon and a phonon must occur in order for both energy and crystal momentum to be conserved. However, in amorphous semiconductors the absence of well defined electron Bloch states leads to a relaxation of the momentum selection rule. For this reason amorphous silicon absorbs light much more strongly than the crystalline form. A thickness of only 2 microns or so is necessary to absorb essentially all incident light of energy greater than the 'band gap', in contrast with the tens of microns needed for a typical single crystal silicon solar cell. Tauc [11] derived an expression for the absorption $\alpha(E)$ assuming no momentum selection rule, which can be written as

$$\alpha(E) = \int_{-\infty}^{\infty} \frac{g(E_1)g(E_1 + E)dE_1}{E} \qquad (3)$$

where $g(E)$ is the density of states at energy E.

Using the assumption that the density of states in the conduction and valence bands is parabolic the equation

$$\alpha(E) = \frac{B}{E}(E - E_0)^2 \qquad (4)$$

where B and E_0 are constants, can be derived. This equation can also be derived by other means [12]. The parameter E_0, the 'Tauc band gap' is widely used (in place of the band gap parameter of crystalline semiconductors) to characterize films. It does not represent a true region of zero density of states but has rather the nature of a fitting parameter.

The result, equation (4) describes the region of the absorption curves for the photon energy range where the absorption is high (α greater than about $10^4 cm^{-1}$ corresponding to about 1.8eV photons), which is the region of interest to us at present. For light of less energy the behavior changes; there is an 'Urbach edge' within which the absorption coefficient varies exponentially with energy; this has been attributed to thermal and structural disorder [13], [14] or to excitonic effects [15], [12]. This region persists for light energies down to about 1.6eV in intrinsic a-Si:H. Careful studies of the absorption or still lower light energies by such methods as photothermal deflection spectroscopy [16] can be used to measure the defect density of states above and below the valence and conduction band mobility edges. Figure 13 shows the absorption coefficient as a function of wavelength as measured by Borsenberger [17].

The Tauc 'band gap', and thereby the light energy at which strong absorption occurs, can be modified by alloying with such elements as germanium (which reduces the gap) or carbon (which increases it.) Such alloying has been used to construct multijunction solar cells with broadened spectral responses and consequent enhanced efficiencies. The photoconductivity of such alloys is however considerably lower than that of device quality a-Si:H. Doping with carbon is also used to raise the band gap and thereby reduce absorption at visible wavelengths in the heavily doped region adjacent to the transparent top electrode. Light absorbed in this layer is effectively wasted owing to the short drift length of photogenerated carriers. In the case of a detector such as we envisage, this p-doped layer may be thicker than that in a conventional solar cell, possibly as thick as 0.1 μm in contrast to the 0.01μm more conventionally used. It will therefore be necessary to increase the band gap of this layer in order to reduce this loss.

3.2 The Photocurrent

For photon energies greater than Ec-Ev, absorption leads primarily to the creation of a mobile electron and hole. In a device consisting of an area of amorphous silicon with ohmic contacts, this can give rise to a constant photocurrent density given by

$$J = Ge\ell_c\left(1 - \exp(-L / \ell_c)\right)$$

In the case of a detector with high reverse bias the drift length can be made much greater than the sample thickness in which case all electron-hole pairs are absorbed; the current density is J=GeL and the charge collected when n photons are absorbed is

$$Q = \eta n e$$

where η, the quantum efficiency, is the number of carrier pairs generated per photon. Charge collection for more general conditions of recombination time and electric field is considered in Sect. 7.

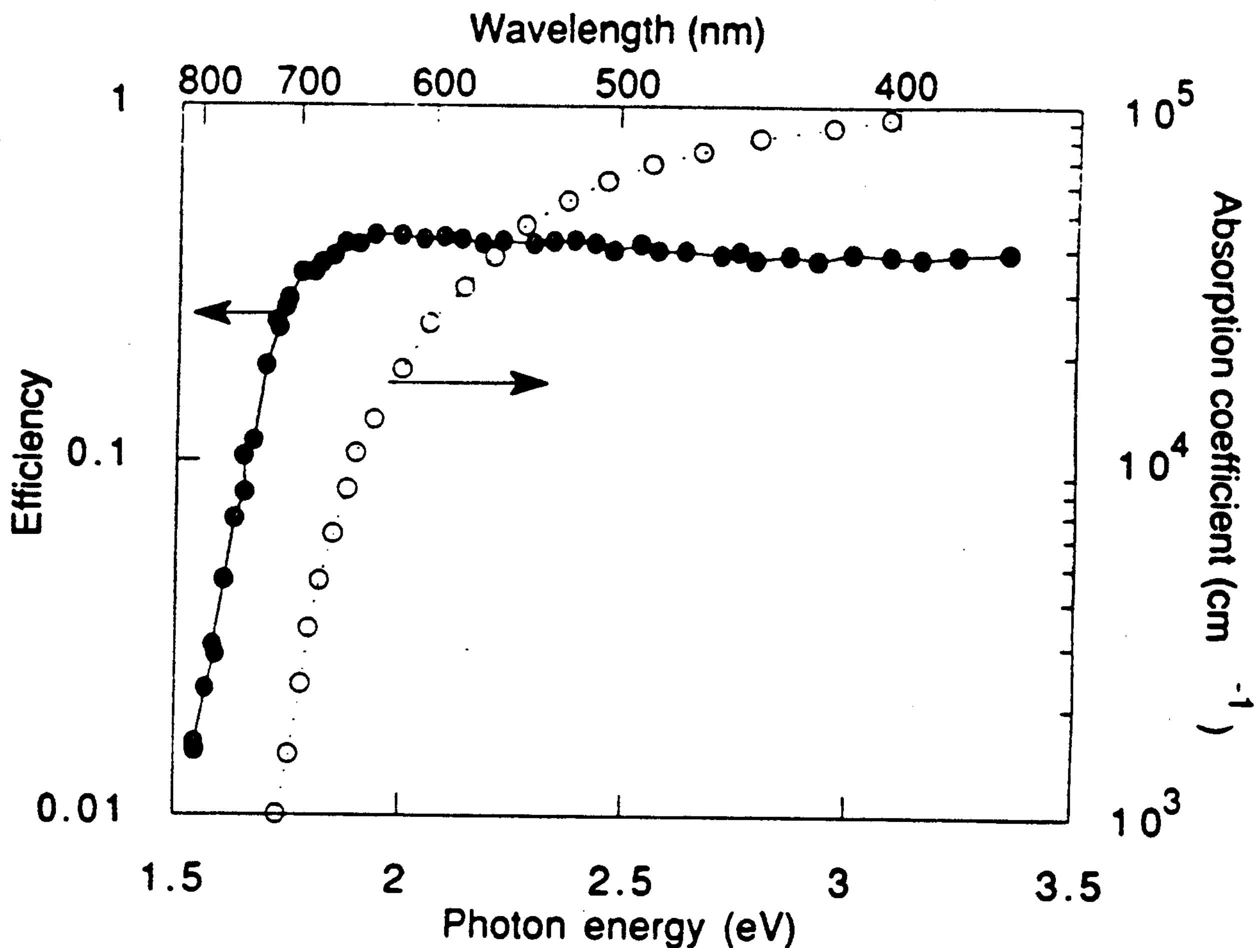

Fig. 13: Absorption mean free path (open circles) and detection efficiency (solid circles) of 11 μm a-Si:H photoreceptor.

3.3 Quantum Efficiency and Choice of Scintillator

The quantum efficiency of a photoconductor can be specified as the number of free electrons (or holes) created per photon absorbed. This figure may be significantly lower than unity if absorption of light can proceed by mechanisms other than electron-hole

generation, or if 'geminate recombination', i.e. recombination of photoexcited pairs immediately after creation, occurs for a significant fraction of pairs. The latter is the case in amorphous semiconductors such as selenium. The quantum efficiency for amorphous Si as measured by Borsenberger [17] is also plotted in Fig. 13. He measured a maximum quantum efficiency of about 40% but this efficiency refers to the entire device, i.e. effects such as surface reflection are not taken into account. This efficiency was found to be constant for light with energy larger than or comparable to the difference between the conduction and valence band mobility edge energies. For light energies below this value one or both of the photogenerated carriers is emitted into a state of low mobility. This increases the probability of geminate recombination, leading to a sharp drop in quantum efficiency. Obviously the scintillator to be used must emit light of an energy corresponding

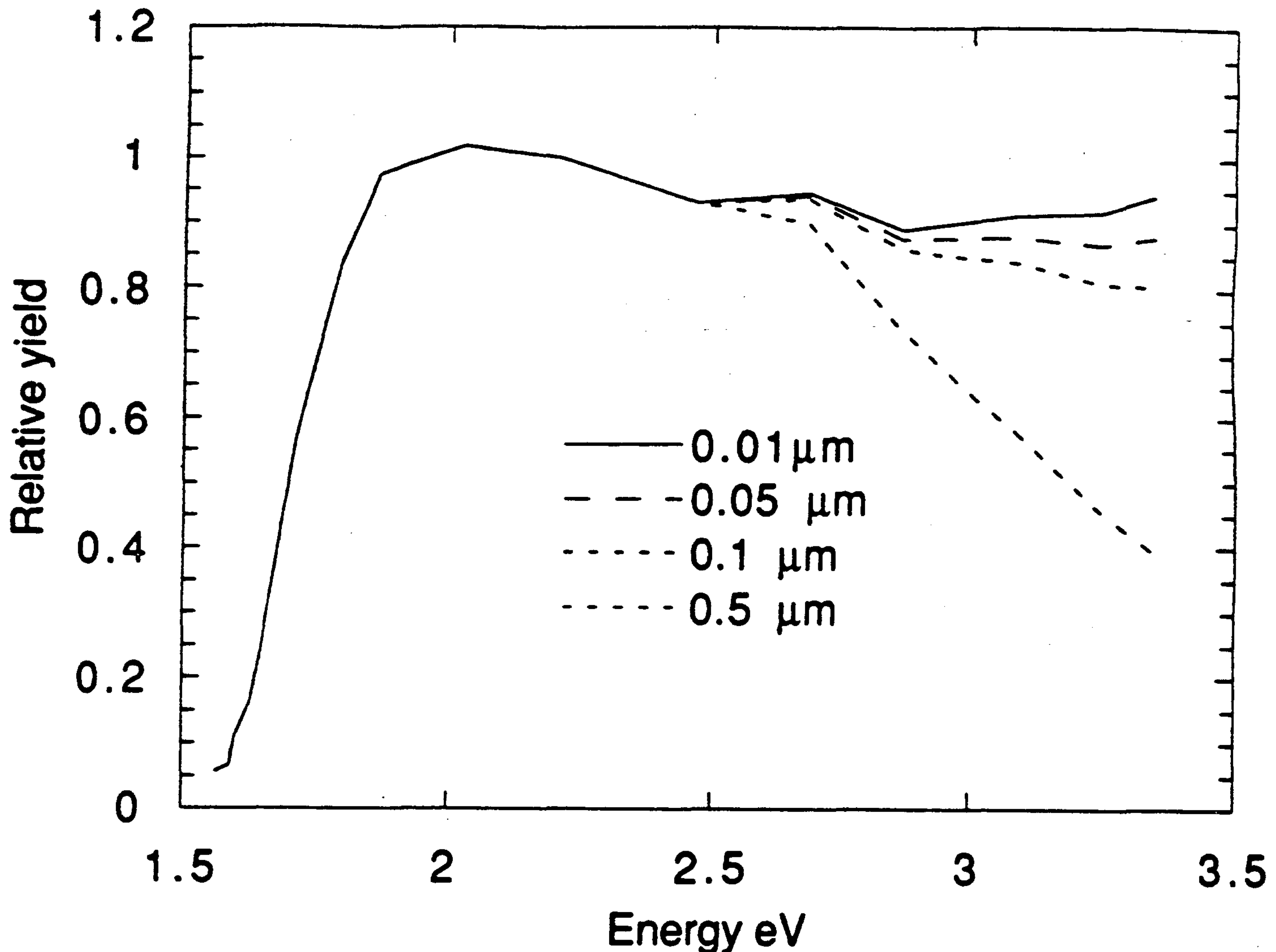

Fig. 14: Normalized detection efficiency of a-Si:H receptor including absorption losses in various *p* layer thicknesses.

to a high quantum efficiency in the detector, that is, of energy greater than the mobility gap. However, light of too high an energy will be so strongly absorbed that much of it will be lost in the heavily doped *p* layer nearest the transparent electrode. As stated above, it is desirable to increase the band gap of the heavily doped layer nearest the transparent contact in order to reduce these losses. Figure 14 shows the product $\eta(E)(1-\exp(-\alpha(E)D))$, where η is the normalized quantum efficiency of the *i* layer and Q is the absorption coefficient, as a function of the light energy E for a range of thicknesses D of the *p* layer. This product gives the expected yield of electron-hole pairs in the intrinsic layer. The band gap in the *p* layer has been taken as 2.5eV which corresponds to a Si_xC_{1-x} alloy with x about 0.5 [18], [19] and the Tauc expression used for the absorption, with absorption parameters taken from Sussmann and Ogden [18]. The quantum efficiency data was taken from Borsenberger [17] and normalized to unity at 2eV. Clearly the predominant photon energy emitted by the scintillator should lie between the band gap values for the alloyed and unalloyed layers for maximum efficiency. For photon energies up to 3.5eV the effect of the *p* layer is rather small for reasonable values of D. Scintillators such as CsI, which emits light in the 1.6 - 3.5eV range, are therefore well suited to use with such detectors.

4 CHARGED PARTICLE DETECTION

In crystal silicon, with the exception of very heavily ionizing charged particles such as fission fragments or very low energy electrons, the charge collected in a reverse biased diode is proportional to the ionization energy deposited in the depletion width of the diode. The charge production mechanism is assumed to be as follows [20]. (a) Pair creation energies are essentially independent of the characteristics of the incident particle. (b) The primary pairs produce secondary pairs and (c) some of the incident energy from the primary and secondary pairs goes into lattice excitation-phonons.

We assume that these basic mechanisms play a similar role in the a-Si:H diodes. Additionally, however, in a-Si:H reverse biased diodes the collected charge is a strong function of the linear energy transfer - dE/dx - of the particles [8], [22], [24] and of the charge collection time (shaping time) of the attached amplifier [21]. These differences are due to the considerably smaller mobilities, diffusion coefficients, and carrier lifetimes of the electrons and holes in the depletion region.

These characteristics are shown in Fig. 15 in which the signals produced by various dE/dx particles are plotted as a function of the charge collection normalized to an equal thickness depletion layer xtal Si diode. The shaping time for these measurements was 2 μsec - which is sufficient for full charge collection in the xtal Si diode. The data for the

low energy protons (1 - 11.6 MeV) [7], [22] and for low energy electrons (5 - 12 KeV) [23] plotted at their corresponding dE/dx point shows that only some fraction of the charge is collected: the remainder is lost due to recombination and limited hole collection at this shaping time. The assumption that there is appreciable charge recombination is made plausible by the data taken at 60° where the sideways component of the electric field separates the *e*, *h* carriers and hence reduces the charge recombination effect [22], [23], [24]. The fact that at 60° the signal collected from the 4 - 11 MeV protons has the same amplitude as that of the 860 MeV alpha particles and of the minimum ionizing 1 MeV electrons implies that recombination effects have essentially been eliminated under these conditions. However, although the calculations of Section 7 show that a xtal Si diode of

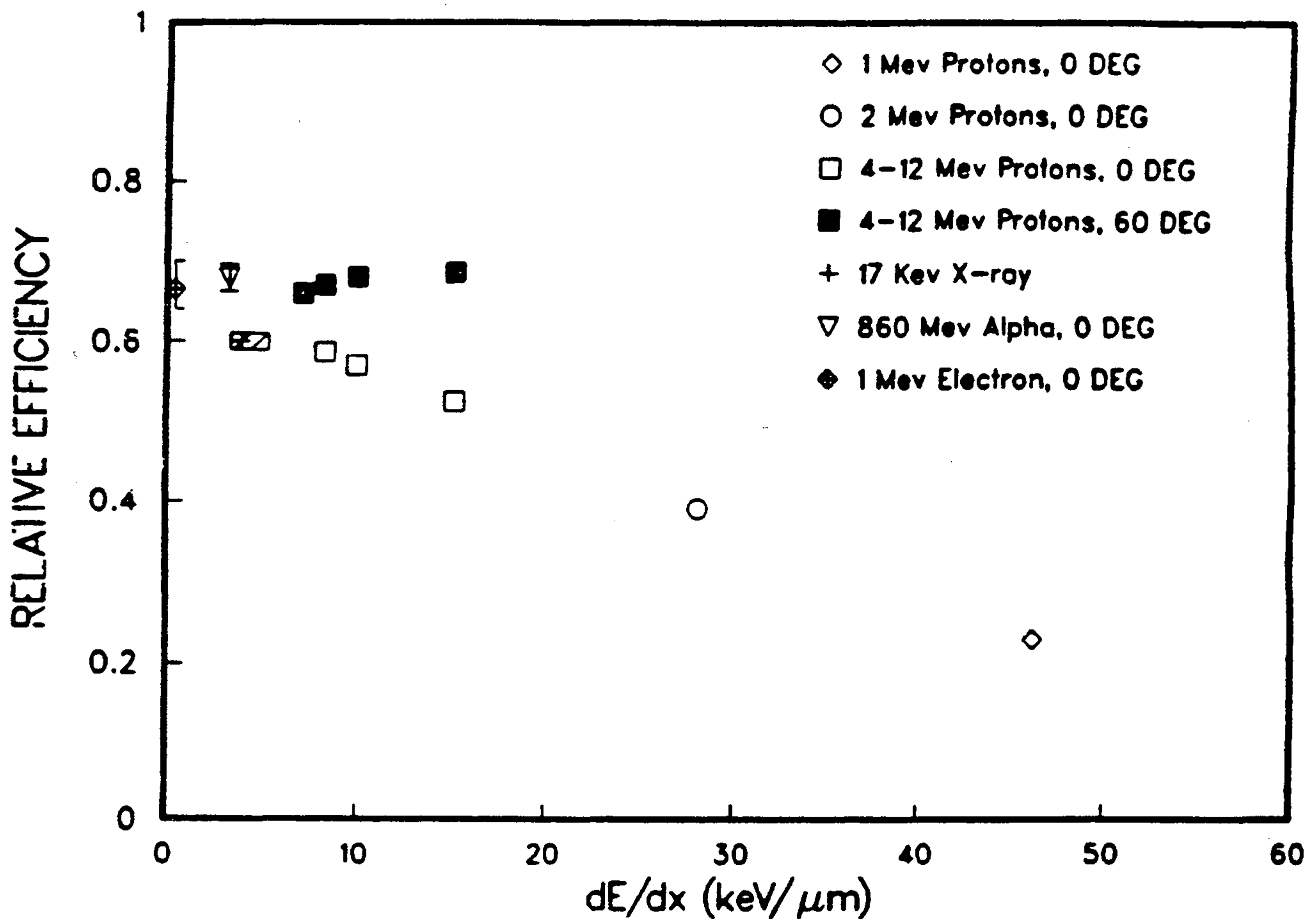

Fig. 15: Signals produced by particles with various values of dE/dx. The 4-12 MeV proton data at 0° and 60° directions is taken from Ref. [7].

comparable thickness would collect the full signal with the 2μsec shaping time, in the a-Si:H there would be a full collection of the electrons only and a partial collection of the holes, due to their low mobilities and small mean free paths [21].

The average energy W required to produce 1 *e,h* pair can be estimated from the data in Fig. 15. For this purpose we use the 860 MeV alpha particle data which has a dE/dx seven times minimum ionizing. The trajectories of these particles are well defined in the a-Si:H detector and traverse it with very little scattering. In a series of measurements, done on a 12.5 µm *p-i-n* diode, the bias voltage was varied as well as the shaping times. After making the necessary corrections for hole capture and losses, the value obtained is W = 4.8 ±0.3 KeV. This number agrees approximately with the empirical relationship of Klein [20] between W and band gap which is

$$W = 2.8 \times \text{Bandgap} + \text{Phonon Loss}$$
$$= 2.8 \times 1.7 + 0.5 = 5.2 \text{ eV}$$

The calculated fraction of the signal charge from fully depleted *p-i-n* diodes as a function of bias is shown in Fig 16 for diodes 12.5 and 29µm thick, and compared to the

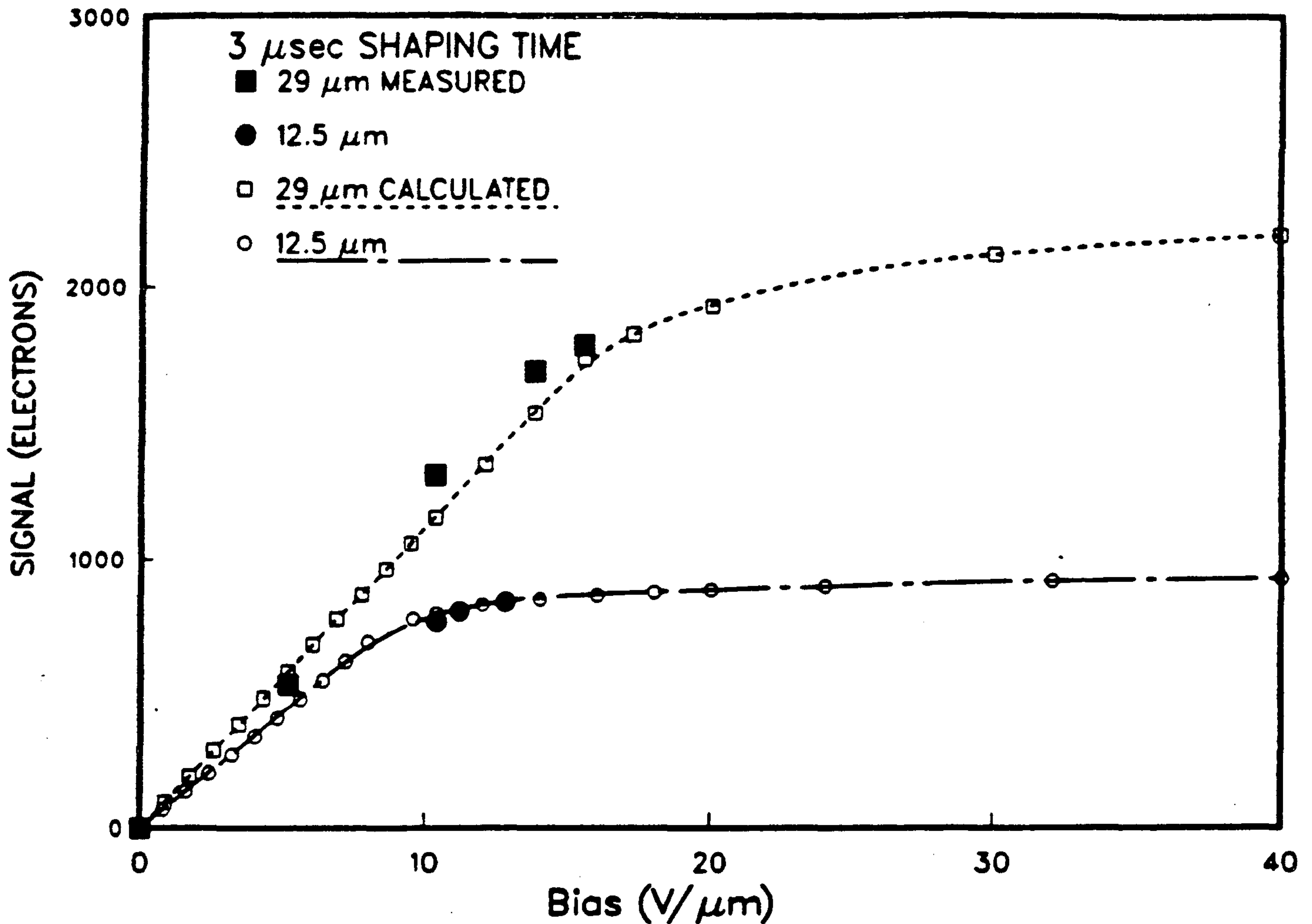

Fig. 16: Signals produced by 1 MeV electrons vs. bias in 12 and 29 µm thick *p-i-n* diodes. Shaping time = 3µsec. Calculated signal is taken using equations of Ref. [21].

signal measured from 1 MeV minimum ionizing electrons. Full depletion bias - as determined from photo diode data similar to that of Fig 4 is assumed. The charge collection curves show that it is possible to collect the electron signal completely over a wide range of shaping times, whereas the hole signal increases with longer shaping times but does not reach the expected limiting value. This is due to the fact that even in the 12μm diode there is some hole capture which becomes appreciably larger for the thicker diodes.

5 DETECTION OF X-RAYS AND γ RAYS

Amorphous silicon diodes are not efficient detectors of x-rays and γ rays unless their energy is extremely low ~ 2 KeV, or less. Even thick *i* layer diodes ~ 100 μm have too low absorption by either photoelectric or Compton interactions. In the energy range from 8 - 17 KeV, which is widely used in x-ray crystallography, a convenient way of enhancing the x-ray conversion efficiency is to use an admixture of a-Si:H with a-Ge:H. The higher Z (32) of germanium increases the conversion efficiency as can be seen from Table 1.

Table 1 Detection Efficiency of a-Si:Ge:H Alloys

	100% Si		90% Si + 10% Ge		80% Si + 20% Ge	
X-ray energy	30 μm	50 μm	30 μm	50 μm	30 μm	50 μm
8 keV	0.37	0.53	0.45	0.63	0.53	0.72
17 keV	0.051	0.083	0.18	0.28	0.31	0.46

The maximum fraction of Ge admixture is taken to be ~ 20% since higher concentrations tend to decrease the mobilities and mean free paths of the free *e,h* carriers in the *i* layer of such a diode to an unacceptable level.

For high energy x-ray or γ ray detection (Eγ >50 KeV) other forms of converters can be used. A scheme utilizing thin tantalum converter layers interspersed between a-Si:H diode layers has been proposed [25] for x-ray flux detection with position sensitivity. The thickness of the tantalum layer, the a-Si:H diodes, and the total number of layers has to be optimized for the specific energy range of the x radiation. This converter scheme has the disadvantage that each a-Si:H layer is independent of the others and hence requires its own bias and signal electronics, which is inconvenient even when using thin film transistor readout.

A third alternative is to use some form of x or γ radiation converter to visible light, for which there are a number of possible selections. First, glass fiber optics plates loaded

with terbium or cerium rare earth scintillators are commercially available [26]. The plate thicknesses are in the range of a few millimeters with fiber diameters down to 20μm. When coupled to a-Si:H pixel diodes with associated TFT electronics these devices can work as high spatial resolution x or γ ray flux detectors which could serve as electronic substitutes for x-ray film. The scintillation light yield in these devices is relatively low because of the low concentration of rare earth in the glass, hence the signal from individual events would be lost in the noise.

For detection of γ rays in the few MeV region and with moderate spatial resolution it is possible to use the image intensifying screens of the type made by Kodak [27] and others for the purpose of enhancing the sensitivity of x-ray film in radiological applications. These intensifying screens are loaded with various rare earth and other fluorescent materials with relatively long > 1 msec decay times. They are presently being used, coupled to thin a-Si:H light sensitive diodes, and to a-Si:H TFT readout electronics as position sensitive (~1mm spatial resolution) radiation monitors for radiation oncology treatments [28].

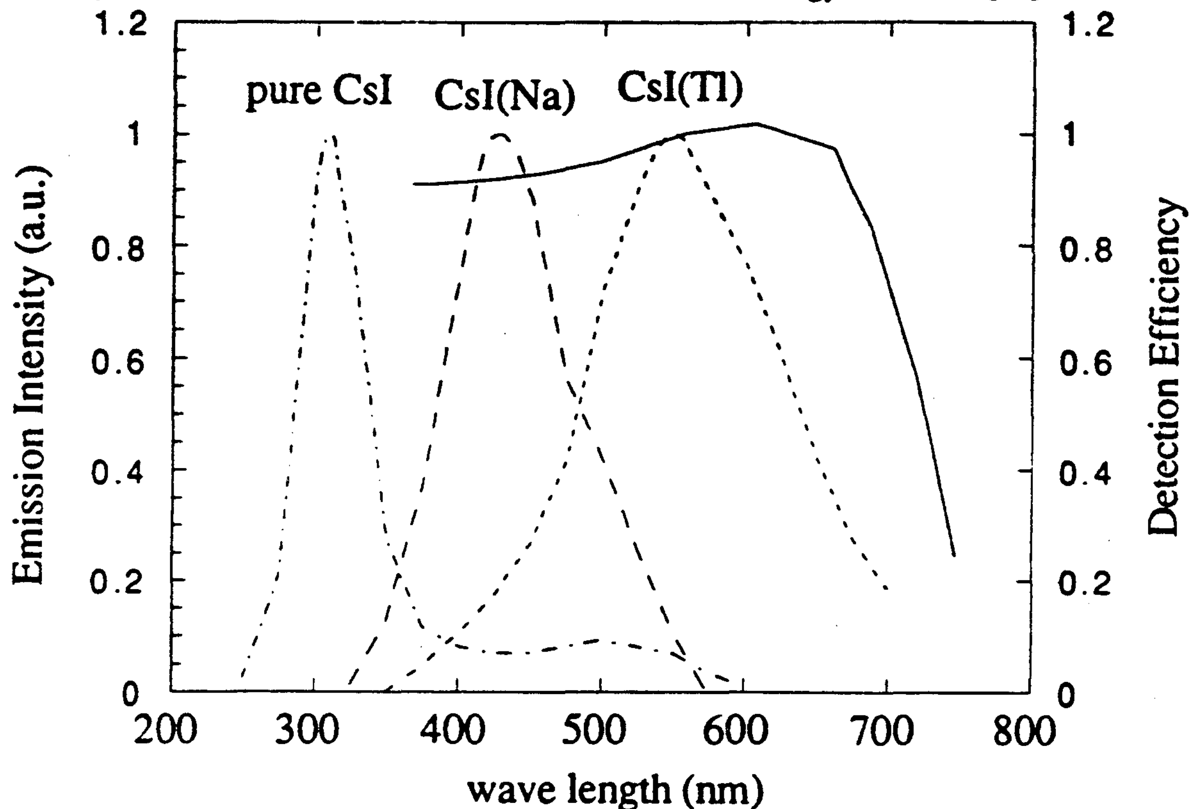

Fig. 17: Scintillation light spectrum of pure, sodium activated and thallium activated cesium iodide. Solid line shows the detection efficiency of 2mm thick a-Si:H diode.

A ceramic scintillator - Gd_2O_2S has been used with a-Si:H diode strips deposited directly on the ceramic for use as the x-ray detector in computerized tomography machines [29], [30].

A very versatile scintillator for use with the a-Si:H photo diode is cesium iodide - pure, sodium activated, or thallium activated. It can be grown in large crystals or it can be vacuum evaporated in thick 300 to 500 μm layers. The light emission spectrum is shown in Fig. 17. For 1 MeV of deposited energy by the incident radiation CsI(Tl) has an integrated light yield of ~ 50,000 photons with a decay period of 1.1 μsec: CsI (Na) has a light yield of 38,000 photons with a decay period of 650 nsec [31]. Pure CsI has a very fast component with a modest light yield (2000 photons: 20 nsec) and some slower components [32]. These CsI scintillators can be used in various applications involving charged particle, γ ray or x-rays in the few KeV to tens of MeV ranges. CsI(Na) has been used commercially as the detection phosphor in x-ray image intensifier tubes [33], deposited by vacuum evaporation at substrate temperatures of 100 - 200°C: hence it can be deposited directly on a-Si:H photodetector diode layers, glass or metallic substrates, with thicknesses in the range of 300 - 500 μm. By selecting appropriate cooling rates the evaporated layers are caused to form thin 20 - 50 μm fibre like channels which collimate the light from the particle, x or γ radiation and thus permit them to be used in high resolution pixel devices [34].

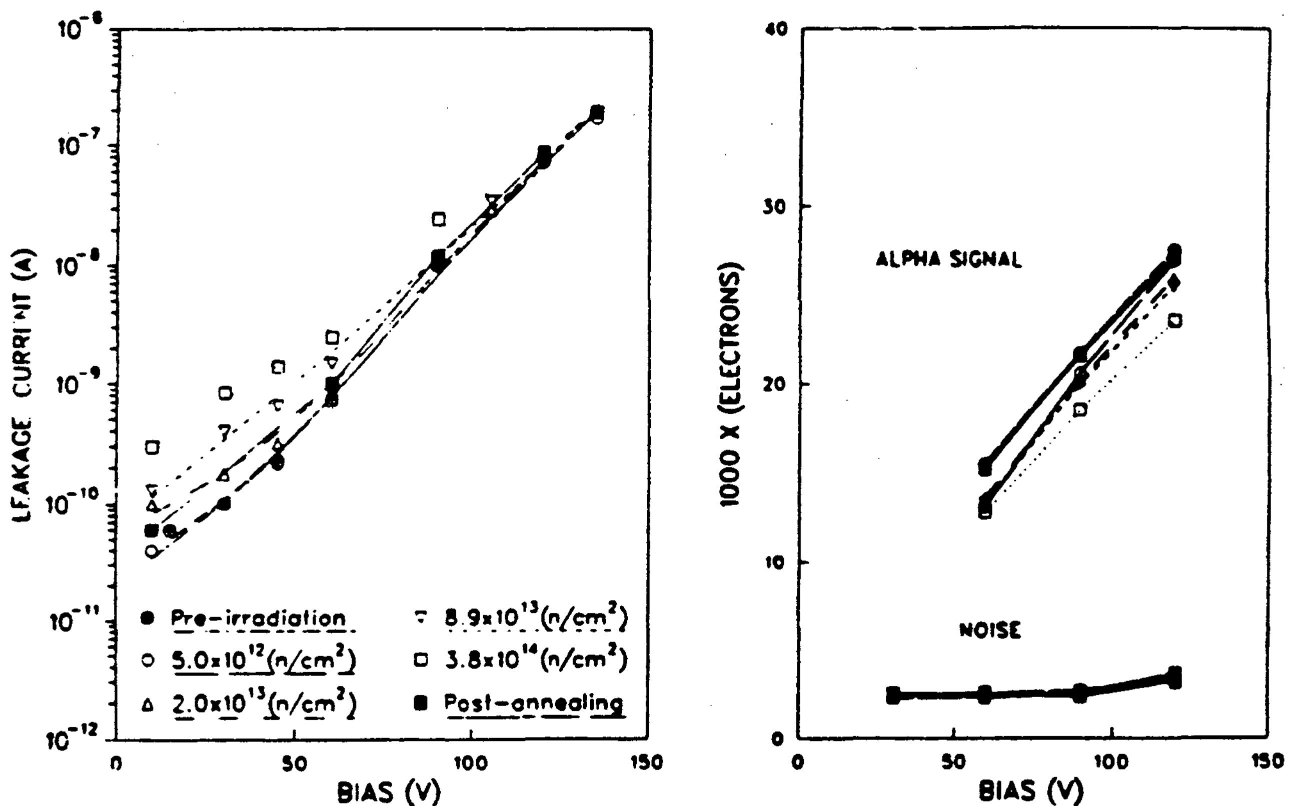

Fig. 18: Radiation damage in a-Si:H diodes induced by 1 - 1.5 MeV neutrons. (a) Radiation induced changes in reverse current before and after annealing. (b) Radiation induced changes in signal and noise.

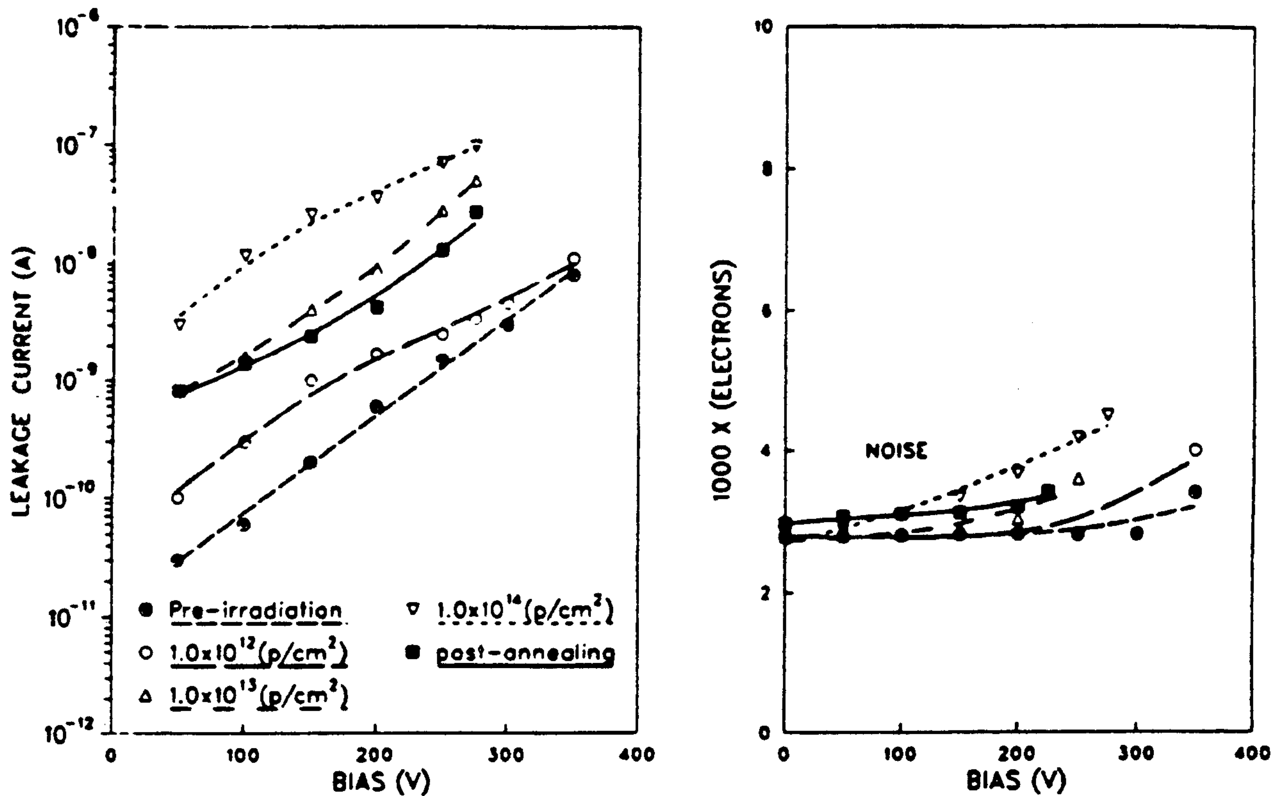

Fig. 19: Radiation damage of a-Si:h diodes induced by 1.5 MeV protons. (a) Radiation induced changes in reverse currents before and after annealing dots. (b) Radiation induced changes in noise before and after annealing.

6 RADIATION RESISTANCE OF A-SI:H *P-I-N* DIODES

Many applications of radiation detectors involve exposure to large fluxes integrated over the useful lifetime of the detector. In the charged particle detector applications discussed in Sect. 7.1 the radiation damage due to energetic neutrons or protons of energies > 1 MeV is expected to be the dominant effect.

The basic phenomena of the radiation damage in xtal silicon and in hydrogenated amorphous silicon is the displacement of Si and H atoms from their sites by the interaction with the incident particles. In a-Si:H this could cause bond breaking. While a neutron has to suffer a knock-on collision to cause such a displacement damage, protons can cause it additionally through a coulomb interaction. At 1.5 MeV incident energy the interaction cross section for neutrons is σ_N ~2.4 barns whereas for protons σ_p ~35000 barns. Thus more displacement damage can be expected in the proton case [36].

A number of *p-i-n* diodes were exposed to ~ 1 MeV neutrons [8] from the fission spectrum of a reactor and to 1.4 MeV protons from an electrostatic accelerator [35], with fluxes ranging from 10^{11} to 10^{14}/cm^2. The resultant radiation effects are shown in Figs 18 and 19.

These data show the following (a) there is some change in the reverse current (b) there is very little change in the noise and (c) there is very little change in the signal amplitude as measured by 6 MeV alpha particles. The main change - increase in reverse current was reduced to pre-irradiation conditions by annealing at 180°C for ~ 2 hours. The fact that there was only a slight increase in noise correlated with the change in leakage current is explained by the observation, shown in Fig. 21 that the current generated noise is a minor contributor to the overall noise at low bias conditions, and with low reverse currents. Radiation damage due to x rays and γ rays has also been studied and shown to be unimportant up to integrated fluxes of ~ 10^{17} 1MeV photons/cm^2 [37].

Radiation damage due to visible light and the Wronski-Staebler effect [38] occurs at intensities considerably higher than would be encountered on our scintillation converter applications.

7 SIGNAL AND NOISE IN A-SI:H DETECTORS

The signal produced in a-Si:H diodes is dependent on the energy deposited in the depletion thickness of the detector layers and on the characteristics of the amplifiers which collect it. The noise generated in conjunction with the signal collection depends also on the detector configuration, on the first stage of the amplifying device, and on the material properties of the diode. Because of the mutual coupling between detector diode and the electronics, it is useful to treat them jointly.

7.1 Signal Characteristics

The signal amplitude can be expressed as a voltage pulse $V = Q/C$ with various modifications. The charge Q is developed in the depleted region of the *i* layer by the incoming radiation. In the case of visible light - from scintillator coupled detectors - there are losses in traversing the metal electrode surfaces and p^+ layers, as shown in Fig. 14. In the case of charged particles producing a number of *e,h* pairs along their trajectory through a thick *i* layer, there could be losses due to charge recombination and electron or hole capture in the material. For both cases the fraction of the charge that is finally collected depends on the amplifier shaping time.

7.2 Signal Collection and Amplifier Characteristics

In this section we discuss amplifier characteristics and their effect on the collected signal amplitude. We assume a detector configuration as shown in Fig. 2. The signal input is $V_i = Q(t) / C$ where $Q(t)$ is the charge reaching the gate electrode of the charge sensitive amplifier stage. The capacitance C is the sum of the detector and TFT capacitances. The signal output of the first stage can be expressed as $V_0 = Q / C_f$ where C_f

is the feedback capacitor and the open loop gain G>>1 [39]. The shaping stage usually has a time invariant configuration of differentiation - CR - followed by one or more stages of integration - $(RC)^n$. A configuration of CR-$(RC)^4$, which is often used, will produce a Gaussian like output with a width of RC sec [40].

The smallness of the hole mobility (0.003 -0.006 $cm^2/Vsec$) compared to that of the electrons (1 - 1.5 $cm^2/Vsec$) results in the fact that it is possible to collect most of the electron signal for shaping times ≥ 20 nsec for *i* layer thicknesses of 2 - 100 μm. A sizeable fraction of the hole signal is lost even for shaping times as long as 10 μsec; the fraction lost increases with *i* layer thickness.

Figure 20 shows the electron and hole signal collection for a range of shaping times. The calculation [21] (see Appendix B) includes the density of dangling bonds, the

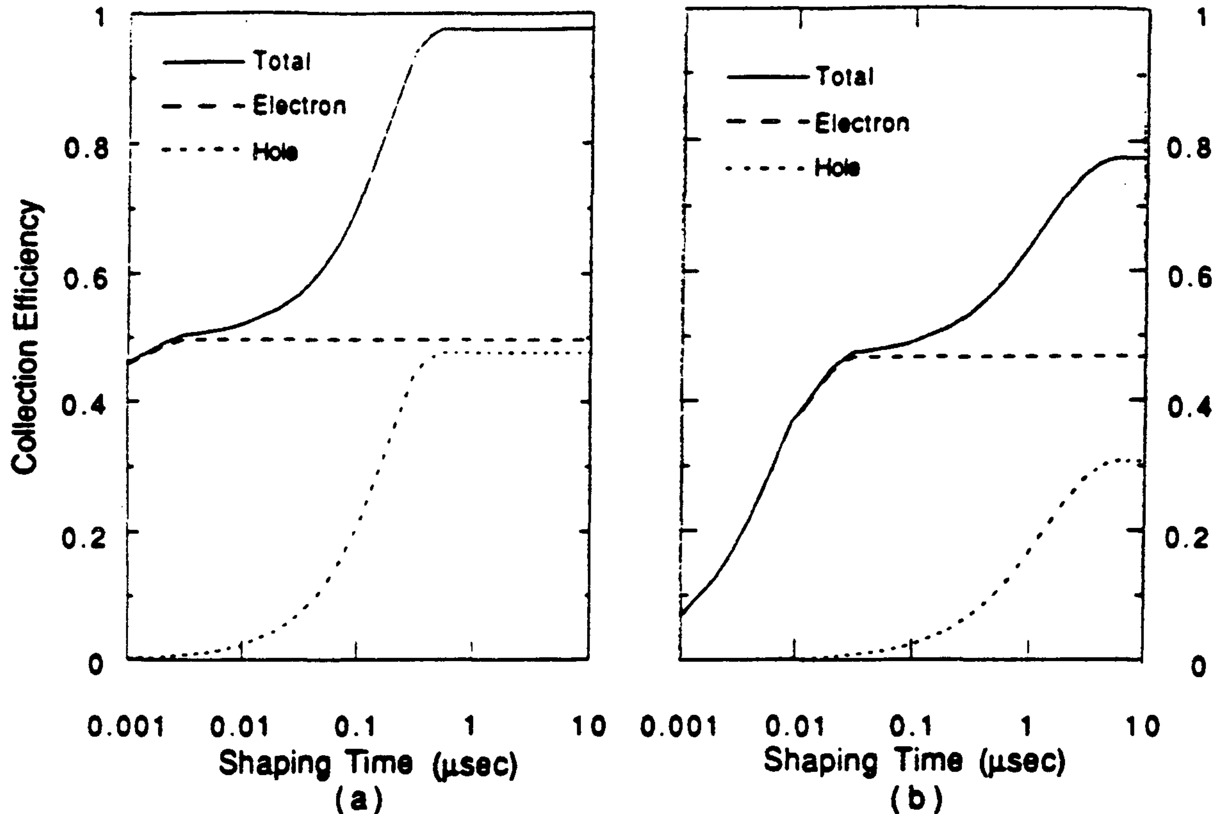

Fig. 20: Calculated electron and hole signal collection vs. shaping time. (a) 5μm thick diode. (b) 50μm thick diode.

related carrier lifetimes, the carrier mobilities, the electric fields, as well as the external bias and the CR - $(RC)^n$ shaping times.

7.3 Noise

In a typical detector configuration as shown in Fig. 2, all the components will generate some noise whose total will limit the minimum signal that can be used. Fig. 21

shows the current and noise generated by a reverse biased *p-i-n* detector 25μm thick, as a function of bias voltage, coupled to a charge sensitive amplifier as shown in Fig. 2.

The following noise sources, shown in Table 2, have previously been associated with xtal Si detectors in this configuration.

Table 2: Noise in Frequency and Time Domain

	Frequency Domain (V^2/Hz)	Time Domain (electrons)	
Nyquist	$v^2 = 4kT\frac{2}{3g_m}\Delta f$	$N^2 = (C_D + C_i)^2 x \frac{e^2 kT}{3q^2 g_m \tau}$	Delta
Shot	$v^2 = \frac{2qI_{Det}}{(C_D + C_i)^2 \varpi^2}\Delta f$	$N^2 = \frac{e^2 I_{Det}\tau}{4q}$	Step
1/f	$v^2 = \frac{K_f}{C_i f}\Delta f$	$N^2 = (C_D + C_i)^2 x \frac{e^2 K_f}{2q^2 C_i}$	1/f

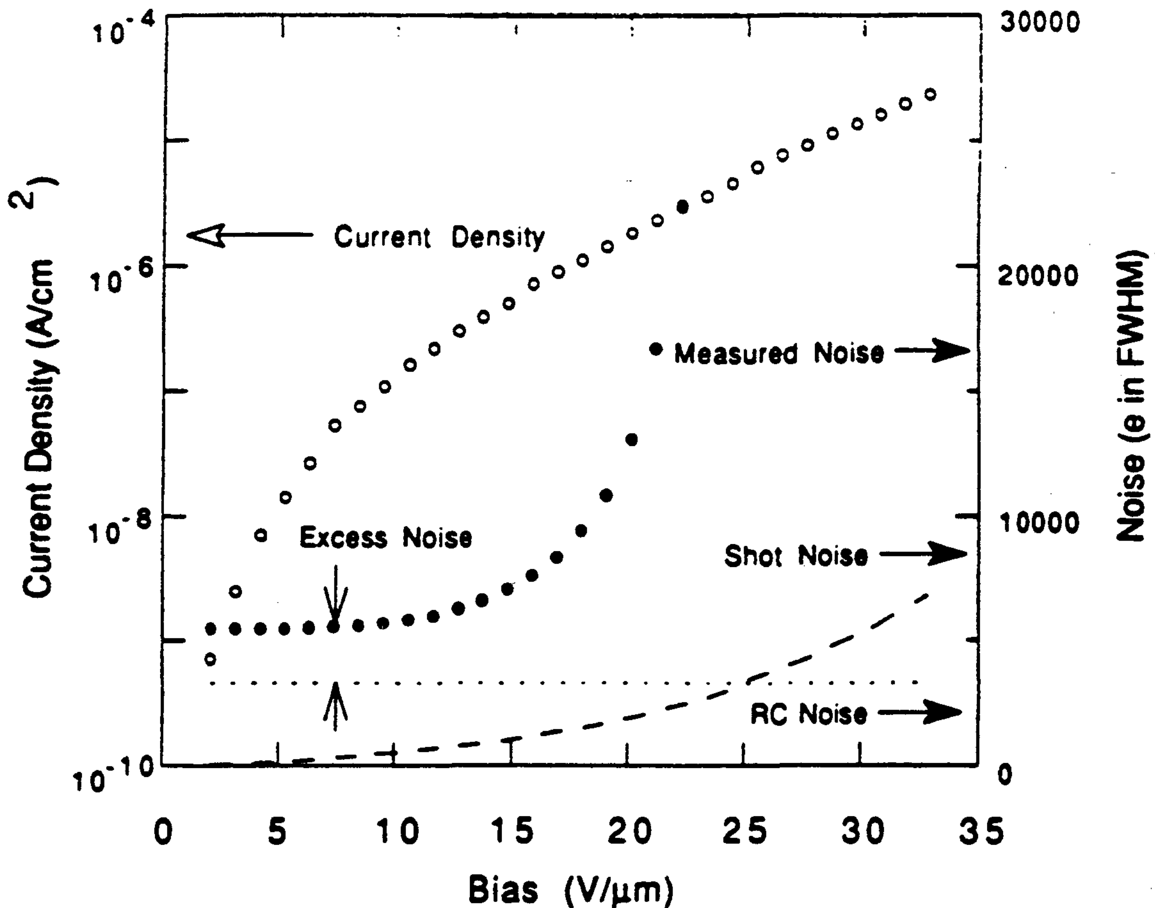

Fig. 21: Reverse current and noise (1μsec shaping time) measured on 25μm thick diode. Noise sources at various biases are shown.

These noise sources are also present in the a-Si:H case, whether coupled to crystal Si field effect transistors (FET), to amorphous silicon, or to polysilicon thin film transistors (TFT). They can be expressed both in the frequency or in the time domain [40], [41]. For detector applications it is usually more convenient to express them in the time domain, for a specific shaping time τ as is done in Fig. 21.

We discuss the following individual noise components as shown here. In the low bias region we have two components; first a Nyquist noise source generated by the bias resistor, by the channel resistance of the detector and by the input stage of the amplifier. When expressed in the time domain as Δ noise it depends on the sum of detector (C_d) and TFT input capacitance (C_i). The remaining noise can be identified as being material generated noise with a 1/f spectrum, hence it is designated as 1/f noise. This noise source is postulated to originate in the fluctuations of the drifted electrons and holes being captured and re-emitted from the tail state distributions [42].

The step noise contribution was calculated from the measured reverse bias current.

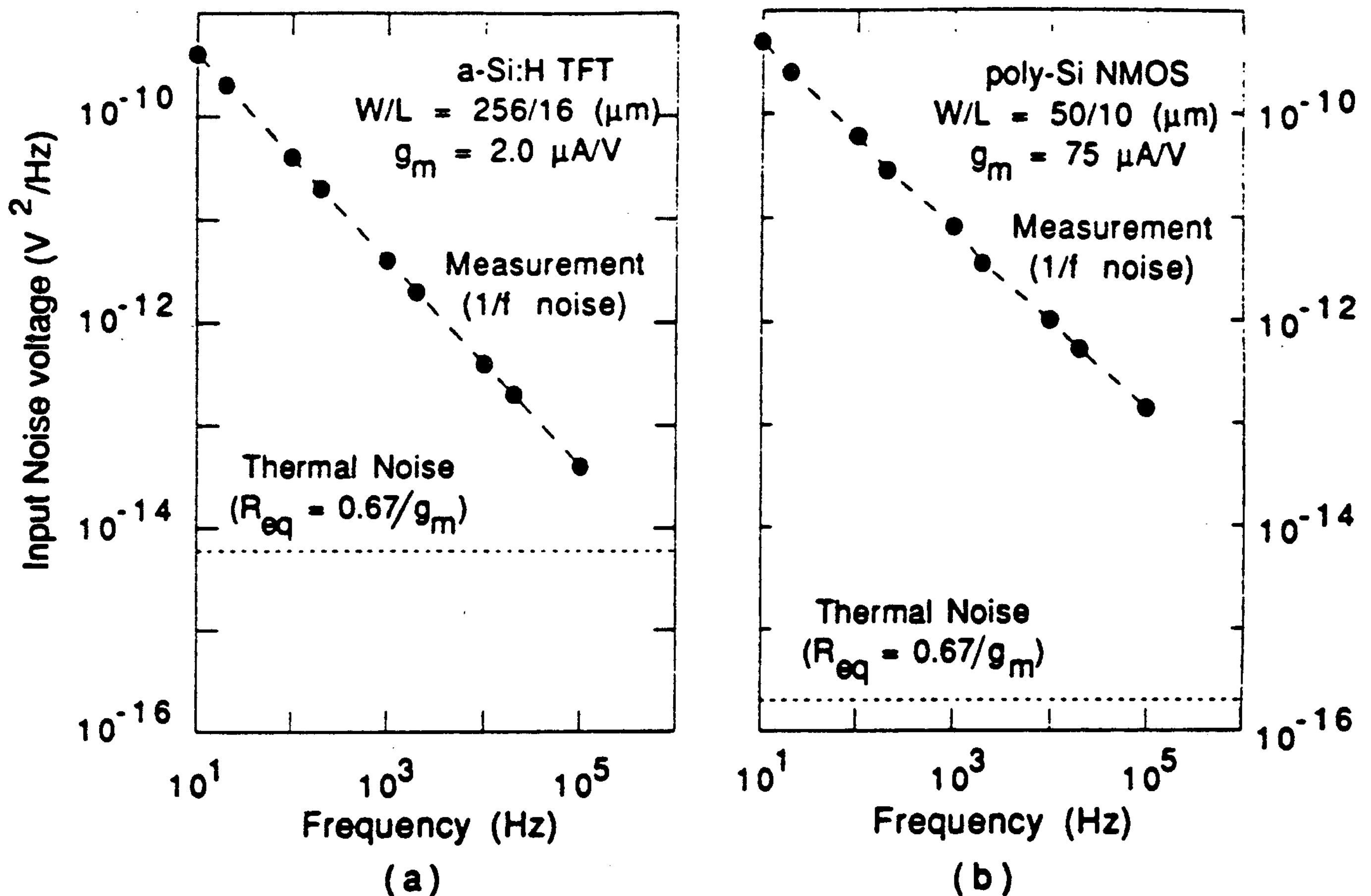

Fig. 22: 1/f and thermal noise. (a) Amorphous silicon TFT. (b) Polysilicon TFT.

From Fig. 21 it can be seen that at low reverse current when the bias is low it is insignificant compared to the other two. At the bias voltage close to the rapid rise in noise, it starts to contribute. The rapid rise in noise seen in all of the detector diodes, is not one of the three noise types discussed here. When observed on an oscilloscope it appears as irregular bursts, indicative of a pre-breakdown condition. This effect has also been identified in xtal Si diodes as "microplasma" breakdown [4], and is believed to originate in irregularities of the metal -p^+ interface [4]. There is some confirmation for this assumption, discussed in Section (2), where we showed that alternative schemes for reducing the electric field at this interface allowed detectors to operate with higher biases.

It is useful here to discuss the noise generated by the input amplifier stage since the use of pixel detectors requires coupling to distributed FET amplifiers of any kind, xtal Si, a-Si:H or polysilicon.

The noise generated by integrated circuit insulated gate field effect transistors can be expressed as [43].

$$\overline{V}^2 = \frac{2}{3} g_m \quad + \frac{k}{C_{ox} W L f^{\alpha}}$$

C_{ox} is the capacitance of the insulator layer. L, W are the length and width of the gate electrode. $\alpha \approx 1$ denotes the 1/f noise and k is the noise constant for the device.

Figures 22 a,b show measurements on a-Si:H and polysilicon TFT noise measured on a shielded probe station. These show that the major noise source up to 1 MH_z is the 1/f component. This noise can be expressed in the time domain as shown in Table 2. A detector - readout amplifier, optimized for minimum noise requires that the input capacitance of the first stage amplifier be made equal to the detector capacitance [40]. If we consider a detector pixel of dimensions ranging from 50 x 50 μm up to 500 x 500 μm,

TABLE 3: Noise in 50x150x150 μm Pixel Detector Coupled to TFT Amplifier

	a-Si:H TFT amp	poly-Si TFT amp
Delta	40	37
Step	48	20
1/f	200	207
Total	209	211
S/N	~10	~10

which is a useful range for many applications, we can plot below the effect of the various noise sources. For example we take a detector with capacitance C_p = amplifier capacitance

= 50fF which corresponds to a pixel size of 150 x 150 μm for a detector 50 μm thick. For other pixel areas and thicknesses these numbers can be scaled using the equations of Table 2.

8 DETECTOR APPLICATIONS

Applications of a-Si:H diodes to light detection are well documented. They include various forms of solar cells, facsimile page readers, flat screen TV devices, electrocopiers and others.

Applications to the detection of charged particles, x-rays and γ rays are new and mostly in the development stage compared to xtal silicon devices and electronics [44]. The

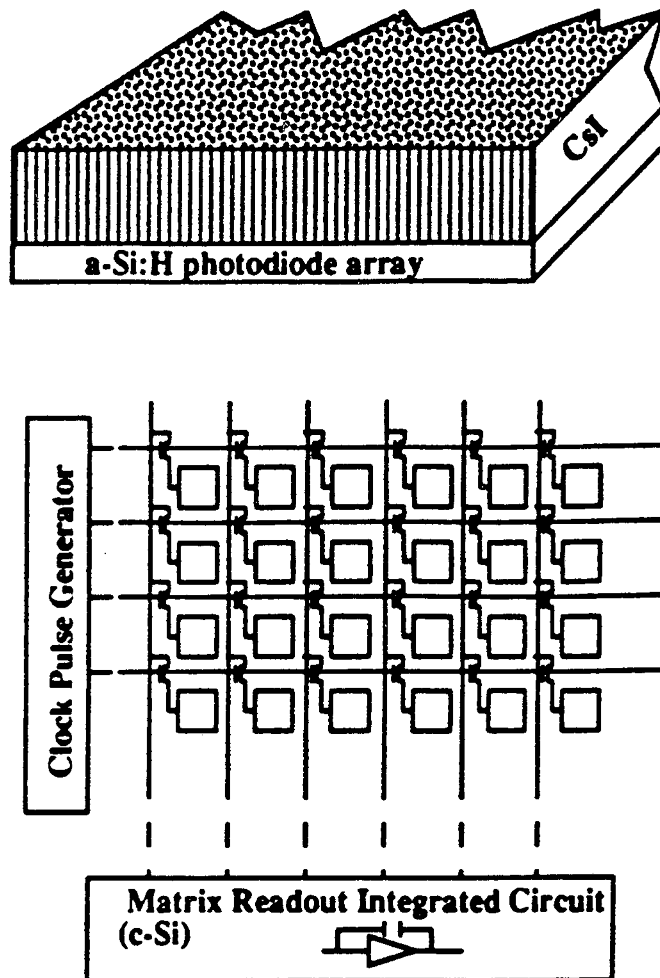

Fig. 23: Schematic of matrix readout for pixel arrays. Amplifier is single TFT for fluences; 3 stage amplifier for single particle detection.

applications described here all require position sensitivity and hence a readout scheme as shown schematically in Fig. 23. For fluence detection the individual pixel amplifier is a

simple charge integrating stage; for single particle detection, the pixel amplifiers would have to be multi-stage devices with a low noise, charge sensitive or voltage input stage.

8.1 Charged Particle Detector Applications - High Energy Physics

These applications require position sensitive detectors capable of detecting individual, minimum ionizing particle distributions. The type of detector can be either one shown in Fig. 1. The thick a-Si:H detector has the advantage that its resistance to radiation damage is considerably larger than the CsI or other scintillators for single particles that might be used in the detection scheme of Fig. 1b.

High energy physics research utilizes position sensitive detector arrays in tracking applications to map out the trajectories of individual particles and thus measure their energy and momentum, and in Calorimeters to measure the energy of γ ray and particle (Hadronic) showers. A schematic example of a tracking array is shown in Fig. 24. Cylindrical rings

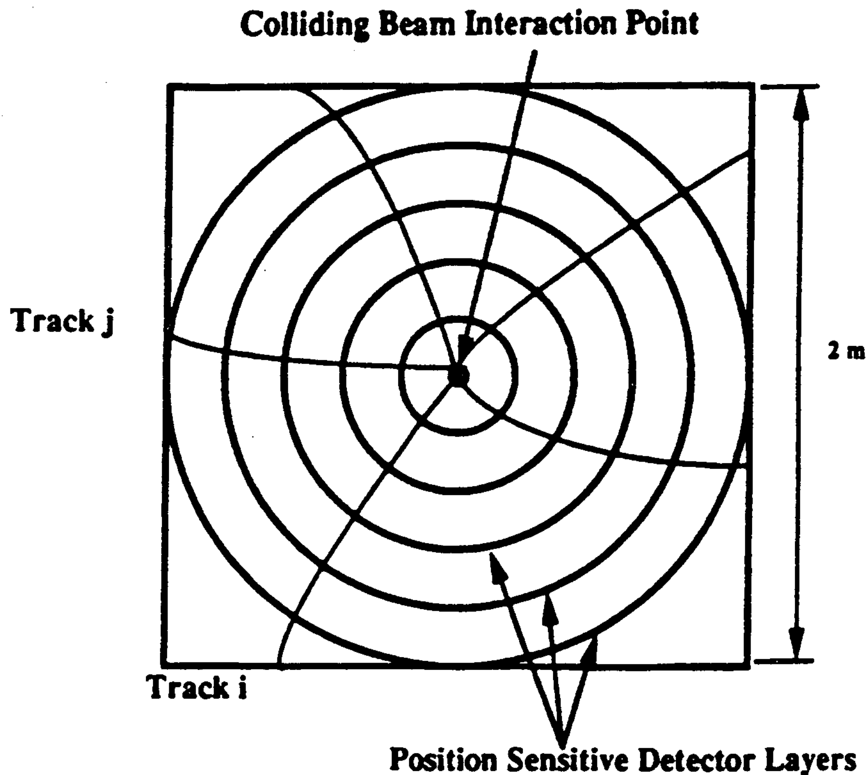

Fig. 24: Schematic of track determining arrays surrounding interaction point of colliding beam accelerator.

of position sensitive layers are placed surrounding the intersection point of a colliding beam accelerator. Strong magnetic fields are used in some detectors, in which case the tracks are curved in the field region. In other detectors without magnetic fields the particle tracks are straight. Because of the high energy the detector arrays are a few meters in diameter have

many tracking layers and have tens of square meter areas. Position accuracy varies from 10 microns near the collision vertex to a few tens of microns at greater distances.

A second application of charged particle position sensitive detector arrays is in γ ray and hadronic calorimeters shown schematically in Fig. 25. The calorimeters typically consist of many lead or uranium plates a few millimeters thick with position sensitive detector array planes between them. A high energy γ ray will produce a cascade of electrons and positrons by interacting with the dense high Z plates. By mapping out the distribution of electrons and positrons through the calorimeter it is possible to determine the

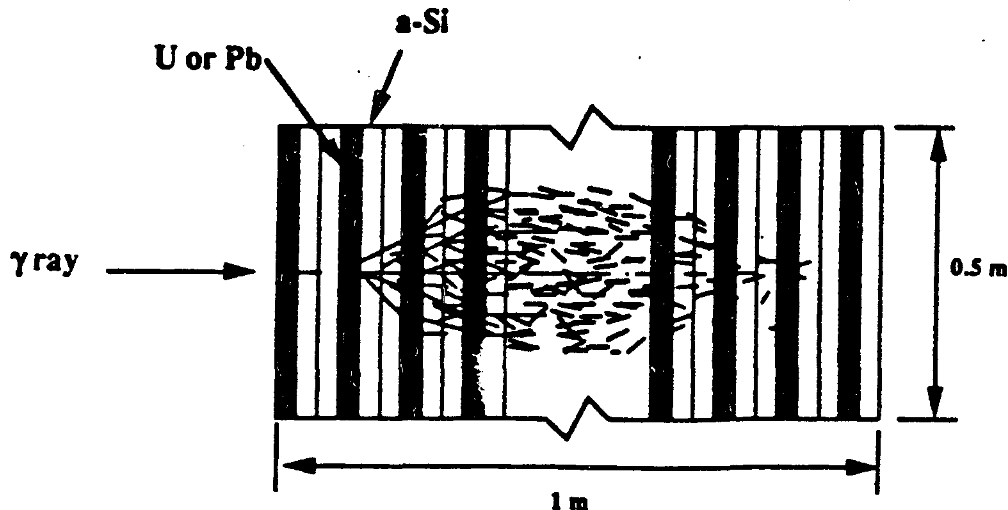

Fig. 25: High energy calorimeter detector. Lead or uranium plates ~5 mm thick with pixel detector planes in between.

energy and direction of the incident γ ray. A similar situation exists with showers induced by high energy hadrons or mesons; the shower components in this case are mostly protons and various types of mesons. High energy calorimeters of this type may have a few hundred square meters of detector area, with pixel sizes ~ 1 - 10 mm.

8.2 Charged Particle Detector Applications - Radionuclide Labelled Chromatography

Radionuclide labelled chromatography is a powerful tool used in biology to trace the distribution of proteins, DNA fragments and other biological complexes. The biological compounds are separated out by their different migration speeds in chromatographic gels by gravity or under the action of electric fields (electrophoresis). The recording may be one dimensional (strip chromatography) or two dimensional (area chromatography).

Radionuclides typically used for labelling are Tritium (E_β = 18 KeV), Phosphorous -32 (E_β = 1.7 MeV), or Sulphur - 35 (E_β = 167 KeV. A strip detector of a-Si:H is shown schematically in Fig. 26 connected to a linear electronic readout. Typical strip dimensions

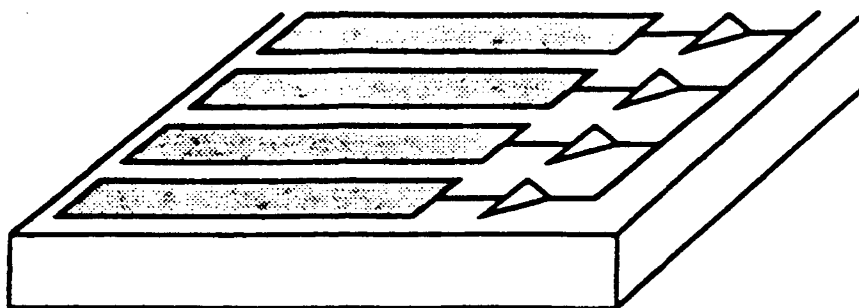

Fig. 26: Strip detector with linear array electronic readout for radionuclide labelled chromatography.

would be 0.1 x 10 mm. The chromatographic plastic gel can be placed over the a-Si:H strips and the distribution of electrons from the labelling radionuclide then determines the position of the various biological fragments and their relative concentrations. Because of the low counting rate, each beta particle has to be recorded individually using the readout scheme of Fig. 23 with low noise multistage amplifiers at each node.

8.3 X-ray Detection: Radiography

Present medical and industrial radiography utilizes film extensively as the position sensitive detector. Film has excellent spatial resolution but no real time capabilities. It is also not very convenient to convert the film image to computer storage. For real time x-ray detection in angiography and in digital radiology, thin CsI cathode, image intensifiers are used; these are bulky and limited in size.

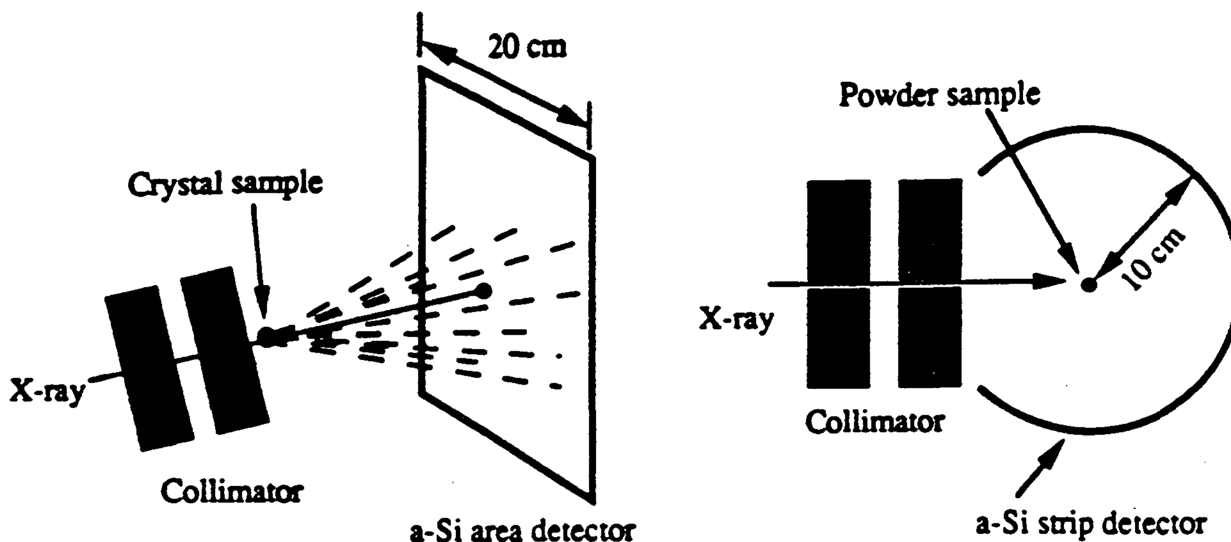

Fig. 27: X-ray crystallography detectors. (a) Area detector with single particle position readout. (b) One dimensional strip detector for powder crystallography.

Position sensitive a-Si:H diode arrays coupled to scintillator - loaded fibre optic face plates or CsI layers are obvious candidates for a real time electronic film substitute. The pixel size required might be 50 to 70 μm. Since large fluences are usually recorded in radiography the position recording electronics need not have low noise signal amplification capability.

8.4 X-ray Detection: Crystallography

X-ray crystallography of single crystals requires that the position as well as the intensity of the diffraction spots be measured. For protein crystallography, where the crystals are small and easily damaged by the radiation , it is advantageous to have a high detection efficiency, electronic, position measuring detector. The individual counts at each diffraction spot are summed up to give the intensity of that diffraction.

X-ray crystallography uses extensively the copper K_α line (8.05 KeV) or the molybdenum K_α line (17.48 KeV). Amorphous silicon diodes with 20 - 30% admixture of a-Ge:H to enhance the sensitivity to these x-rays as shown in Table 1 could be used in

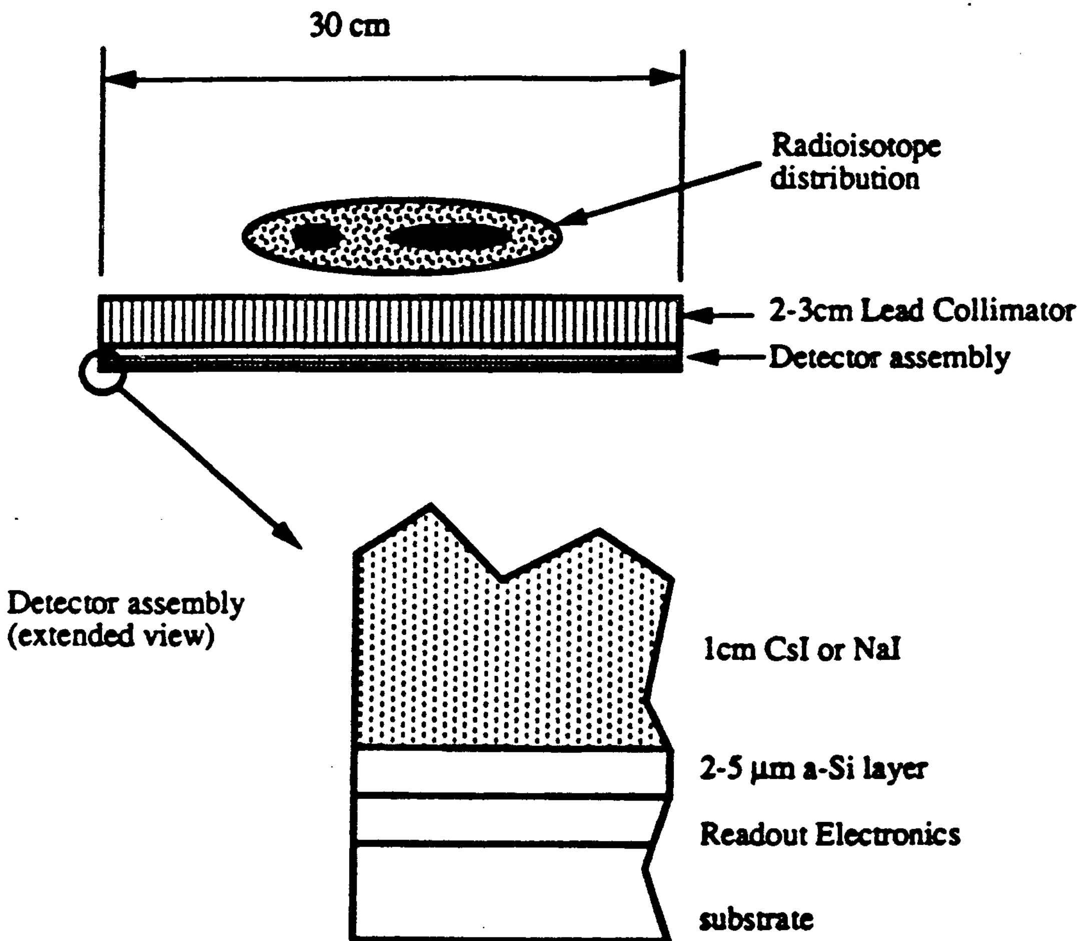

Fig. 28: Schematic of CsI scintillator converter coupled to a-Si:H pixel diode array for detection of single γ distribution.

sources is less than 10^5/sec, each event would have to be amplified and recorded separately using distributed TFT low noise charge sensitive amplifiers.

Another crystallography application - to record the patterns from powder or multicrystal samples can use a one dimensional strip detector curved on the arc of a circle to record a large fraction of the scattering angle pattern as shown in Fig. 27b.

For x-ray applications in real time from a synchrotron light source accelerator where the event rate is high, integrated fluences could be measured both in the 2D and in the 1D configurations.

8.5 Single γ Ray Detection

A useful application could be to nuclear medicine where it is necessary to measure the distribution of γ rays (70 KeV - 360 KeV) originating from patients organs in which a suitably compounded γ emitting isotope has been injected. Present imaging devices utilize large diameter (up to 60 cm) sodium iodide scintillator single crystals viewed by an array of photomultipliers. The position of each gamma ray landing on the crystal is determined by microcomputer circuits which receive the signal from a number of adjacent photomultiplier tubes and determine the centroid of the signal, thus locating the γ position to an accuracy of 3 - 4 mm. The photomultiplier array (~60 separate P-M tubes) can be replaced by a a-Si:H layer with pixel areas of ~ 2 mm as shown in Fig. 28. In this case also, because of the low count rate ($<10^5$/sec), the position of individual events has to be recorded separately, with ancillary low noise TFT electronics.

Acknowledgements

One of us (Victor Perez-Mendez,) would like to thank J. Kanicki (IBM Thomas Watson Research Center) for inviting him to write this report as a chapter in his forthcoming book, "Physics and Applications of Amorphous and Microcrystalline Semiconductor Devices" (Artech Press, Boston). We would like to thank A. Madan, co-editor of the MRS Symposium Proceedings on Amorphous Silicon Technology for various suggestions. Thanks are due to C. C. Tsai (Xerox), P. Bhat, J. Xi (Glasstech-Solar), J. Coleman (Plasma Physics) for making various a-Si:H diodes.

This work was supported by the Director, Office of Energy Research, Office of High Energy and Nuclear Physics, Division of High Energy Physics, of the U.S. Department of Energy under Contract No. DE-AC03-76SF00098.

References

1. Cohen, J.D., "Density of States from Junction Measurements in Hydrogenated Amorphous Silicon," Semiconductors and Semimetals, Vol. 21, Part C, 1984, pp. 9 - 16.

2. Kaplan, S.N., J. R. Morel, T. A. Mulera, V. Perez-Mendez, G. Schlurmacher, R. A. Street, "Detection of Charged Particles in Amorphous Silicon Layers", IEEE Trans. Nuc. Sci. NS 33 (1986), pp. 351-354.

3. Qureshi, S., V. Perez-Mendez, S. N. Kaplan, I. Fujieda, G. Cho and R. A. Street, "Material Parameters in a Thick Hydrogenated Amorphous Silicon Detector and Their Effect on Signal Collection," Mat. Res. Soc. Symp. Proc. Vol. 149, 1989, pp. 649 - 654.

4. Rose, D. J., "Microplasmas in Silicon", Phys. Rev. 105 1957, pp. 413-418.

5. Fujieda, I., G. Cho, M. Conti, J. Drewery, S. N. Kaplan, V. Perez-Mendez, S. Qureshi and R. A. Street, "Improved Charge Collection of the Buried p-i-n a-Si:H Radiation Detectors," to be presented at IEEE Nuclear Science Symposium, San Francisco, CA, Jan 17 - 19, 1990.

6. Stutzman, M., D. K. Biegelsen and R. A. Street, "Detailed Investigation of Doping in Hydrogenated Amorphous Silicon and Germanium," Phys. Rev. B, 35, 1987, pp. 5666-5701.

7. Pochet, T., J. Dubeau, L. A. Hamel, B. Equer, and A. Karar, "Charge Collection in a-Si:H Particle Detectors," Mat. Res. Soc. Symp. Proc., Vol. 149, 1989, pp. 661-666.

8. Perez-Mendez, V., S. N. Kaplan, G. Cho, I. Fujieda, S. Qureshi, W. Ward and R. A. Street, "Hydrogenated Amorphous Silicon Pixel Detectors for Minimum Ionizing Particles," Nucl. Instr. and Meth. A273, 1988, pp.127-134.

9. Street, R. A., J. Zesch, and M. J. L. Thompson, "Effects of Doping on Transport and Deep Trapping in Hydrogenated Amorphous Silicon", Appl. Phys. Lett. 43, 1983, pp. 672-674.

10. Fujieda, I., G. Cho, M. Conti, J. Drewery, S. N. Kaplan, V. Perez-Mendez, S. Qureshi, D. Wildermuth, and R. A. Street, "Field Profile Tailoring in a-Si:H Radiation Detectors," to be presented at Spring Meeting of Mat. Res. Soc., San Francisco, CA May, 1990.

11. Tauc, J. in "The Optical Properties of Solids," (ed. Abeles), (Amsterdam: North Holland), 1970, pp.277-307.

12. Mott, N. F. and E. A. Davis, "Electronic Processes in Non Crystalline Materials," 2nd edition (Oxford: Oxford University Press) (1980).

13. Cody, G. D., T. Tiedje, B. Abeles, B. Brooks, and Y. Goldstein, "Disorder and the Optical Absorption Edge of Hydrogenated Amorphous Silicon," Phys. Rev. Letters. 47, 1981, pp. 1480-1483.

14. Cohen, M. H., C. M. Soukoulis, and E. N. Economou, "Optical Absorption in Amorphous Semiconductors," J. Non-crystalline solids 77 & 78, 1985, pp. 171-174.

15. Dow, J. D., and D. Redfield, "Electroabsorption in Semiconductors: The Xcitonic Absorption Edge," Phys. Rev. B 1, 1970, pp.3358-3371.

16. Jackson, W. B., and N. M. Amer, "Direct Measurement of Gap-state Absorption in Hydrogenated Amorphous Silicon by Photothermal Deflection Spectroscopy," Phys. Rev. B 25, 1982, pp. 5559-5562.

17. Borsenberger, P.M., "Spectral Sensitization of Amorphous silicon by Bromoindium Phthalocyanine;" J. Appl. Phys. 62, 1987, pp.2942-2945.

18. Sussmann, R. S. and R. Ogden, "Photoluminessence and Optical Properties of Plasma-deposited Amorphous Si_xC_{1-x} Alloys," Phil Mag. B44, 1981, pp. 137-158.

19. Tawada, Y. K. Tsuge, M. Kondo, H. Okamato, and Y. Hamakawa, "Properties and Structure of a-SiC:H for High-Efficiency a-Si solar Cell," J. Appl Phys. 53, 1982, pp. 5273-5281.

20. Klein, C. A., "Band Gap Dependence and Related Features of Radiation Ionization Energies in Semiconductors," J. App. Phys. 39, 1968, pp. 2029-2038.

21. Kaplan, S. N., G. Cho, J. Drewery, I. Fujieda, V. Perez-Mendez, S. Qureshi, and R. A. Street, "Signal Generation from the Transit of a High-Energy Ionizing Particle Through an a-Si:H Diode," to be presented at Spring Meeting of Mat. Res. Soc., San Francisco, CA, May 1990.

22. Perez-Mendez, V., S. N. Kaplan, W. Ward, S. Qureshi, R. A. Street, "Signal, Recombination Effects and Noise in a-Si:H Detectors," Nuc. Inst. & Methods, A 260, 1987, pp. 195 - 200.

23. Kaplan, S. N., I. Fujieda, V. Perez-Mendez, S. Qureshi, W. Ward and R. A. Street, "Detection of Minimum Ionizing Particles in Hydrogenated Amorphous Silicon," Nucl. Instr. and Methods A273, 1988, pp. 611-614.

24. Equer, B. and A. Karar, Effect of Primary Ionization in Amorphous Silicon Detectors, Nucl. Instr. and Methods, A271, 1988, pp. 574-584.

25. Naruse, Y. and T. Hatayama, "Metal/Amorphous Silicon Multilayer Radiation Detectors," IEEE Trans. Nucl. Sci NS - 36, 1989, pp. 1347 - 1352.

26. Synergistic Detector Design, 2438 Wyandotte St., Mountain View, CA 94043 Collimated Holes, 460 Division St., Campbell, CA 95008

27. Chronex and Lanex Screens, Eastman Kodak, Rochester, N.Y.

28. Antonuk, L. E., C. F. Wild, J. Boundry, J. Jimenez, M. J. Longo and R. A. Street, "Development of Hydrogenated Amorphous Silicon Sensors for High Energy Photon Radiography Imaging," to be presented at IEEE Nuclear Science Symposium, San Francisco, CA Jan., 1990.

29. Itoh, H., S. Matsubara, T. Talcahashi, T. Shinada and H. Takeuchi, "Integrated Radiation Detectors with a-Si Photodiodes on Ceramic Scintillators," Jap. Jour. App. Physics 28 1989, pp. 1476-1479.

30. Mochiki, K. K. Hasegawa and S. Namatame, "Amorphous Silicon Position-Sensitive Detector," Nucl, Instr. and Meth. A273 1988, pp. 640.

31. Holl, I., E. Lorenz and G. Mageras, "A Measurement of the Light Yield of Some Common Inorganic Scintillators," IEEE Trans. Nucl. Sci. NS-35, 1988, pp. 105 - 109.

32. Kubota, S., S. Sakuragi, S. Hashimoto and J. Ruan, "A New Scintillation Material: Pure CsI with 10ns Decay Time," Nucl. Instr. and Meth. A268, 1988, pp. 275-277.

33. Bates, C. W., "Scintillation Process in thin films of CsI(Na) and CsI(Tl) due to Low Energy X-rays, Electrons and Protons," Adv. Electronics and Electron Physics 28A, 1968, pp. 451-459.

34. Stevens, A. L. N. and A. D. M. Schrama de Paum, "Vapor-Deposited CsI:Na Layers, 1. Morphologic and Crystallographic Properties," Philips Res. Repts 29, 1974, pp. 340-362.

35. Qureshi, S., G. Cho, J. Drewery, I. Fujieda, S. N. Kaplan, V. Perez-Mendez, and R. A. Street, "Radiation Induced Effects in a-Si:H Radiation Detectors and TFT's," to be presented at Spring Meeting of Mat. Res. Soc., San Francisco, CA 1990.

36. Tada, H.Y., J. R. Carter, B.E. Anspaugh, and R. G. Downing, "Solar Cell Radiation Handbook," 1982, pp. (3) 6 - 15.

37. Imagawa O., K. Yasuda, A. Yoshida, "Gamma-ray Irradiation Effect in Amorphous Hydrogenated Silicon," J. Appl. Phys. 66 (10), 1989, pp. 4719-4722.

38. Staebler, D. L., and C. R. Wronski, " Reversible Conductivity Changes in Discharge-Produced Amorphous Si," Appl. Phys. Lett. 31, 1977, pp. 292-294.

39. Kowalski, E., "Nuclear electronics, Springer-Verlag Publishers, pp. 38, New York, 1970.

40. Goulding, F. S. and D. A. Landis, "Signal Processing for Semiconductor Detectors," IEEE Transactions on Nucl. Science, NS-29, 1982, pp. 1125-1141.

41. Radeka, V., "Signal, Noise and Resolution in Position Sensitive Detectors," IEEE Trans. Nuc. Sci. NS-21, 1974, pp. 51-64.

42. Bathaei, F. Z. and J. C. Anderson, "Electrical Noise Measurements in Intrinsic Amorphous Silicon," Phil. Mag. B, 55, 1987, pp. 87-100.

43. Gray, P. R. and R. G. Meyer, "Analysis and Design of Analog Integrated Circuits," John Wiley and Sons, (2nd Edition), pp. 666, New York, 1984.

44. Fujieda, I., G. Cho, S. N. Kaplan, V. Perez-Mendez, S. Qureshi and R. A. Street, "Applications of a-Si:H Radiation Detectors," presented at the International Conference on Amorphous Semiconductor Technology, Asheville, NC, Aug. 1989. J. Non-crystalline Solids 115 (1989) 174-176.

Appendix A

ELECTRIC FIELD DISTRIBUTION IN THE INTRINSIC LAYER OF REVERSE BIASED AMORPHOUS SILICON PIN DETECTOR

A.1 PARTIAL DEPLETION

A.1.1 DEEP AND PARTIAL DEPLETION MODEL (2-REGION MODEL)

When a pin detector is biased at a lower voltage than the required for full depletion of the whole i-layer, the i-layer is divided into two regions depending on the space charge density profile. Region I is called the deep depletion region where the space charge density is constant. Region II is the partially depleted region where the space charge density is approximately proportional to the Fermi energy level shift. The one-dimensional Poisson equations for the two regions are

$$\frac{d^2V(x)}{dx^2} = \frac{-\rho_o}{\varepsilon\varepsilon_o} \qquad 0 \le x \le w$$

$$\frac{d^2V(x)}{dx^2} = \frac{-\rho_o}{\varepsilon\varepsilon_o} \times \left|\frac{V(x)}{V_c}\right| \qquad w \le x \le d$$

where w is the boundary position between the two regions, d is the i-layer thickness, ρ_o is the maximum space charge density of the i-layer due to ionized dangling bonds, and V_c is the maximum shift of the intrinsic Fermi energy level in the i-layer which is about 1 Volt. The boundary conditions for the above coupled differential equations are

$$V_I(\, x=0\,) = -V_a$$

$$V_I(\, x=w\,) = -V_c$$

$$V_{II}(\, x=d\,) = 0.0$$

$$E_I(\, x=w\,) = E_{II}(\, x=w\,)$$

where $-V_a$ is the applied DC bias voltage on the p-contact (x=0) when the n-contact (x=d) is grounded. The subscript refers to the corresponding region. The electric field distribution for regions I and II is found by solving the Poisson equations with the above boundary conditions, and has a solution

$$E(x) = \frac{V_c\,(x - w)}{L^2} - \frac{\frac{V_c}{L}}{\tanh\left[\frac{(d - w)}{L}\right]} \qquad 0 \le x \le w$$

$$E(x) = -\frac{V_c}{L} \times \frac{\cosh\left[\frac{(d - x)}{L}\right]}{\sinh\left[\frac{(d - w)}{L}\right]} \qquad w \le x \le d$$

where L is defined by

$$L \equiv \sqrt{\frac{\varepsilon\varepsilon_o V_c}{\rho_o}}$$

Finally w is determined numerically by the following relation

$$\frac{V_a - V_c}{V_c} = \frac{w^2}{2L^2} + \frac{\frac{w}{L}}{\tanh\left[\frac{(d - w)}{L}\right]}$$

A.1.2 ABRUPT DEPLETION MODEL (1-REGION MODEL)

If we neglect the partial depletion region for region II, the solution of the electric field distribution becomes much simpler than that shown above. We have to solve the Poisson equation for region I only.

$$\frac{d^2V(x)}{dx^2} = \frac{-\rho_o}{\varepsilon\varepsilon_o} \qquad 0 \le x \le w$$

The boundary conditions are

$$V(x=0) = -V_a$$

$$V(x=w) = 0.0$$

$$E(x=w) = 0.0$$

The third condition is required to find w, the depletion width, which is

$$w = \sqrt{\frac{2\varepsilon\varepsilon_o V_a}{\rho_o}}$$

Finally the electric field distribution is

$$E(x) = \frac{\rho_o}{\varepsilon\varepsilon_o}(x - w) \qquad 0 \le x \le w$$

$$E(x) = 0.0 \qquad w \le x \le d$$

A.2 FULL DEPLETION

When the i-layer of an amorphous silicon pin detector is over fully depleted, the electric field in the i-layer is easily calculated by solving the Poisson equation:

$$\frac{d^2V(x)}{dx^2} = \frac{-\rho_o}{\varepsilon\varepsilon_o} \qquad 0 \le x \le d$$

The boundary conditions are

$$V(x=0) = -V_a$$

$$V(x=d) = 0.0$$

The electric field distribution in the i-layer is

$$E(x) = \frac{\rho_o}{\varepsilon\varepsilon_o}x - \frac{\rho_o}{2\varepsilon\varepsilon_o}d - \frac{V_a}{d} \qquad 0 \le x \le d$$

Appendix B

CHARGE COLLECTION EFFICIENCY IN A REVERSE BIASED AMORPHOUS SILICON PIN DETECTOR

The loss of signal charge during the collection process is mainly due to the finite integration time of the electronics and to the trapping and recombination of the charge carriers. For the case of negligible recombination of charge carriers, we develop the collection efficiency in a reverse biased detector for both the partial depletion and the full depletion bias cases. In the partial depletion case, the abrupt depletion model is used. Also the uniform generation of charge carriers by the incident radiation is assumed for both cases.

Define a dimensionless bias, Y, by

$$Y \equiv \frac{V_a}{V_d}$$

where V_a is the applied bias, V_d is the critical bias for full depletion of the detector of thickness d defined as $V_d \equiv \frac{\rho_o d^2}{2\varepsilon\varepsilon_o}$. The electric field for the partial depletion case (A.1.2) and the full depletion case (A.2) are

$$E(x) = \frac{\rho_o}{\varepsilon\varepsilon_o}(x - W) \qquad 0 \le x \le W \qquad (Y \le 1 \text{ ; partial depletion})$$

$$E(x) = \frac{\rho_o}{\varepsilon\varepsilon_o}\left(x - \frac{d}{2} - \frac{W^2}{2d}\right) \qquad 0 \le x \le d \qquad (Y \ge 1 \text{ ; full depletion})$$

where W is defined as

$$W \equiv \sqrt{\frac{2\varepsilon\varepsilon_o V_a}{\rho_o}}$$

When $V_a < V_d$, W becomes the depletion width, w, defined in A.1.2.

B.1 PARTIAL DEPLETION

B.1.1 ELECTRON COLLECTION EFFICIENCY

In a partial depletion case, the generated electrons drift from the p-contact toward the depletion boundary, W. The drift velocity of the charge carrier in the semiconductor is linearly proportional to the electric field, to a first order approximation, so the velocity of an

electron at position x will be given by the following equation by using the electric field distribution for the partial depletion case.

$$v_e(x) = -\mu_e E(x) = \frac{W - x}{\tau_n}$$

where τ_n is the electron characteristic time defined by

$$\tau_n \equiv \frac{\varepsilon\varepsilon_o}{\rho_o \mu_e}$$

Using the definition of the drift velocity for the electron, $v_e(x) \equiv \frac{dx}{dt}$, this can be represented as a function of time, t, and the initial position, x_o, instead of the present position, x.

$$v_e(x_o,t) = \frac{(W - x_o)}{\tau_n} e^{-\frac{t}{\tau_n}}$$

The transit time of the electron from x_o to W is infinite; Theoretically the electron never reaches the position W. This is true for any electron between x_o=0 and x_o=W. In the case of uniform generation of charge carriers, the induced current density due to n electrons generated at x_o is

$$j_e(x_o,t) = q\, n\, e^{-\frac{t}{\tau_\varepsilon}} v_e(x_o,t)$$

where τ_ε is the electron lifetime and the exponential term is a correction factor due to the the loss of electrons by deep trapping. Consider now the charge collection using an ideal charge sensitive preamplifier which is simply a current integrator having a collection or integration time t. The induced charge per unit area of the electrode due to the n electrons generated at x_o, is

$$\Delta Q_e(x_o,t) = \int_0^t j_e(x_o,t')\, dt'$$

The total induced charge due to electrons generated in the depletion region (0 £ x £W) is

$$Q_e(t) = \int_0^W \Delta Q_e(x_o,t) \frac{dx_o}{d} = \int_0^W \frac{dx_o}{d} \int_0^t j_e(x_o,t')\, dt'$$

Since there is no field in the undepleted region, there is no contribution to the signal from carriers in this region. The maximum induced charge per unit area of the electrode by collecting all the electrons in the detector is

$$Q_o = q\,n\,d$$

So the electron collection efficiency, the relative signal size contributed by the electrons is

$$\eta_e(t) \equiv \frac{Q_e}{Q_o} = \frac{Y}{2} \times \frac{1 - e^{-\alpha_e t}}{\alpha_e \tau_n}$$

where

$$\alpha_e \equiv \frac{\tau_n + \tau_e}{\tau_n \tau_e}$$

B.1.2 HOLE COLLECTION EFFICIENCY

Similarly, the drift velocity for holes is

$$v_h(x) = \mu_h E(x) = \frac{x - W}{\tau_p}$$

where τ_p is the hole characteristic time defined by

$$\tau_p \equiv \frac{\varepsilon \varepsilon_o}{\rho_o \mu_h}$$

Using the same process as for the electrons, the velocity of holes at x is represented by the initial position x_o, and the time t.

$$v_h(x_o,t) = \frac{x_o - W}{\tau_p} e^{\frac{t}{\tau_p}}$$

The difference in collection process of holes with electrons is that the electrons can never reach the depletion boundary, W, for any given collection time, t, but some of holes can arrive at the p-contact. Therefore the above velocity expression is only true under the condition that

$$t < t_p \equiv \tau_p \ln\left(\frac{W}{W - x_o}\right)$$

where t_p is the transit time of the holes from x_o to $x = 0$. The current density is also limited up to t_p

$$j_h(x_o,t) = -q\, n\, e^{-\frac{t}{\tau_h}}\, v_h(x_o,t)\, H(t_p - t)$$

where t_h is the hole lifetime and H(t) is the Heaviside function. If the collection time, t, is specified, then a division should be made between two groups of holes; one group consists of the holes which are collected completely during that time and the other consists of the holes which remain in the i layer at time t. The boundary between the initial positions of the two groups of holes is

$$x_p = W\,(1 - e^{-\frac{t}{\tau_p}})$$

The induced charge per unit area of the electrode by collection of holes is

$$Q_h(t) = \int_0^{x_p} \frac{dx_o}{d} \int_0^{t_p} dt'\, j_h(x_o,t') + \int_{x_p}^{W} \frac{dx_o}{d} \int_0^{t} dt'\, j_h(x_o,t')$$

So the collection efficiency contributed by holes is

$$\eta_h(t) \equiv \frac{Q_h}{Q_o} = \frac{Y}{2} \times \frac{1 - e^{-\alpha_h t}}{\alpha_h\, \tau_p}$$

where

$$\alpha_h \equiv \frac{\tau_p + \tau_h}{\tau_p\, \tau_h}$$

B.1.3 TOTAL COLLECTION EFFICIENCY

Finally the total collection efficiency for both electrons and holes in a partially depleted detector for a given integration time t, is

$$\eta(t) = \eta_e(t) + \eta_h(t) = \frac{Y}{2} \times \left[\frac{1 - e^{-\alpha_e t}}{\alpha_e\, \tau_n} + \frac{1 - e^{-\alpha_h t}}{\alpha_h\, \tau_p}\right]$$

B.2 FULL DEPLETION

B.2.1 ELECTRON COLLECTION EFFICIENCY

The procedure for calculating the collection efficiency for the full depletion case is the same as for the partial depletion case except we need to compare the collection time, t, and the maximum transit time, t_n, which is the electron travel time from x=0 to x=d given by

$$t_n \equiv \tau_n \ln\left(\frac{Y+1}{Y-1}\right)$$

If $t < t_n$, then the electron collection efficiency is

$$\eta_e(t) = \frac{1}{8}\left[(Y+1)^2 \frac{1 - e^{-\alpha_e t}}{\alpha_e \tau_n} - (Y-1)^2 \frac{1 - e^{-\beta_e t}}{\beta_e \tau_n}\right]$$

where

$$\beta_e \equiv \frac{\tau_n - \tau_e}{\tau_n \tau_e}$$

If $t \geq t_n$, then the collection efficiency is constant, $\eta_e(t_n)$

B.2.2 HOLE COLLECTION EFFICIENCY

Similarly, if $t < t_p$, then the hole collection efficiency is

$$\eta_h(t) = \frac{1}{8}\left[(Y+1)^2 \frac{1 - e^{-\alpha_h t}}{\alpha_h \tau_p} - (Y-1)^2 \frac{1 - e^{-\beta_h t}}{\beta_h \tau_p}\right]$$

when

$$t < t_p \equiv \tau_p \ln\left(\frac{Y+1}{Y-1}\right)$$

where

$$\beta_h \equiv \frac{\tau_p - \tau_h}{\tau_p \tau_h}$$

If $t \geq t_p$, then the collection efficiency is constant, $\eta_h(t_p)$.

B.2.3 TOTAL COLLECTION EFFICIENCY

The total collection efficiency for a fully depleted detector is

$$\eta(t) = \frac{1}{8}\left[(Y+1)^2 \frac{1 - e^{-\alpha_e t'}}{\alpha_e \tau_n} - (Y-1)^2 \frac{1 - e^{-\beta_e t'}}{\beta_e \tau_n} + (Y+1)^2 \frac{1 - e^{-\alpha_h t''}}{\alpha_h \tau_p} - (Y-1)^2 \frac{1 - e^{-\beta_h t''}}{\beta_h \tau_p}\right]$$

where t' is the minimum value between t and t_n. Also t'' is the minimum value between t and t_p.

LAWRENCE BERKELEY LABORATORY
UNIVERSITY OF CALIFORNIA
INFORMATION RESOURCES DEPARTMENT
1 CYCLOTRON ROAD
BERKELEY, CALIFORNIA 94720